Chapter 3
Normal Contact Problems with Axially-Symmetric Bodies Without Adhesion

Valentin L. Popov and Markus Heß

3.1 Mapping of Three-Dimensional Contact Problems onto One Dimension: The Basic Idea

The *method of dimensionality reduction* is based on the observation that certain types of three-dimensional contacts can be *exactly* mapped to one-dimensional linearly elastic foundations. Even one of the simplest contact problems offers us a taste of this method: If a flat cylindrical indenter is pressed into the surface of an elastic half-space (Fig. 3.1a), then the normal stiffness of the contact is *proportional to its diameter D*:

$$k_z = DE^*, \tag{3.1}$$

where E^* is the effective Young's modulus and is calculated from

$$\frac{1}{E^*} = \frac{1-\nu_1^2}{E_1} + \frac{1-\nu_2^2}{E_2}, \tag{3.2}$$

using the Young's moduli of the contacting bodies E_1 and E_2 as well as their shear moduli ν_1 and ν_2.[1] The proportionality of the stiffness to the diameter can also be reproduced quite trivially by a *one-dimensional* linearly elastic foundation.

The linearly elastic foundation (Fig. 3.1b) is a series of independent, identical springs that are fixed to a rigid substrate separated from one another by a distance of Δx. In order to represent continua, the "discretization step" Δx must, of course, be sufficiently small, which we always silently imply. The number of springs that are in contact with the indenter is equal to $D/\Delta x$. If we denote the stiffness of a single spring as Δk_z, then the total stiffness of the contact is

$$k_z = \Delta k_z \frac{D}{\Delta x}. \tag{3.3}$$

[1] This result can be found in any book dealing with contact mechanics (see, for example [1]).

V.L. Popov and M. Heß, *Method of Dimensionality Reduction in Contact Mechanics and Friction*, DOI 10.1007/978-3-642-53876-6_3

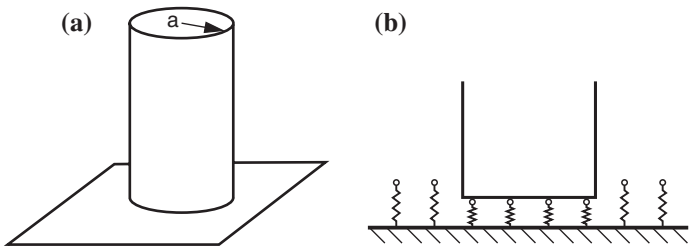

Fig. 3.1 (**a**) Contact between a flat, cylindrical indenter and an elastic half-space and (**b**) the one-dimensional model

In order for Eq. (3.1) to also be valid for the indentation into a linearly elastic foundation, the stiffness per unit length must be chosen to be equal to effective modulus E^*:

$$\frac{\Delta k_z}{\Delta x} = E^*. \tag{3.4}$$

According to this, the stiffness of every individual spring is

$$\Delta k_z = E^* \Delta x. \tag{3.5}$$

The proportionality of the stiffness to the diameter of the indenter is then met rather trivially in the case of an elastic foundation. In the following, it will be shown that the defined elastic foundation is also suitable for the mapping of a large number of other contact problems.

3.2 The Rules of Geike and Popov and the Rules of Heß for Normal Contact Problems

The relationship between normal force, the indention depth, and the contact radius can be reproduced exactly for a broad range of profiles by the reduced contact problem of a one-dimensional linearly elastic foundation. Thereby, the surface profile must merely be modified according to a few simple rules.

Let us first consider the contact between an elastic sphere with the radius R and an elastic half-space (the Herzian contact problem, Fig. 3.2a).[2] As early as 2005, Popov pointed out in a lecture[3] that also for a sphere (or a parabolic indenter) the relationship between normal force, the indentation depth, and the contact radius

[2] Strictly speaking, a parabolic profile with the radius of curvature R is considered.

[3] German–Russian Workshop "Numerical simulation methods in tribology: possibilities and limitations", Berlin University of Technology, March 14–17, 2005. Published in [2].

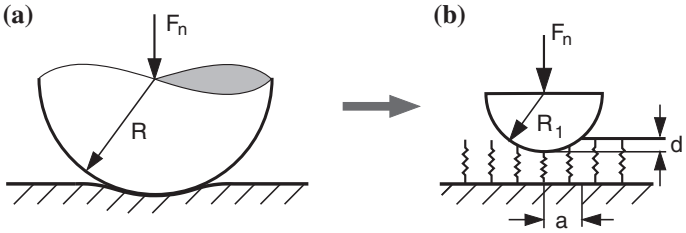

Fig. 3.2 (**a**) Contact between a sphere and an elastic half-space and (**b**) the one-dimensional model

can be *exactly* described by a one-dimensional model (Fig. 3.2b), provided that the radius is scaled by a factor of 1/2. At this point, we will describe the solution for a sphere in detail. In the following chapters, however, we will dispense with the details of the calculation due to their simplicity and only state the results.

The one-dimensional substitution profile should have the radius of curvature of R_1 and is given by the equation

$$\tilde{z} = g(x) = \frac{x^2}{2R_1}. \tag{3.6}$$

If this profile is pressed into the elastic foundation to a depth of d, then we obtain the vertical displacement of the foundation at the point x:

$$u_z(x) = d - g(x) = d - \frac{x^2}{2R_1}. \tag{3.7}$$

The semi-span of the contact area (the "contact radius") a is given by requiring that $u_z(a) = 0$ and is

$$a = \sqrt{2R_1 d}. \tag{3.8}$$

The contribution of a single spring with a coordinate x to the normal force is

$$f_N = \Delta k_z \cdot u_z(x) = E^* \left(d - \frac{x^2}{2R_1} \right) \Delta x. \tag{3.9}$$

The total normal force is obtained by integration over the contact area:

$$F_N = \int_{-a}^{a} E^* \left(d - \frac{x^2}{2R_1} \right) dx = \int_{-\sqrt{2R_1 d}}^{\sqrt{2R_1 d}} E^* \left(d - \frac{x^2}{2R_1} \right) dx = \frac{4\sqrt{2}E^*}{3} \sqrt{R_1 d^3}. \tag{3.10}$$

If we now choose the radius of the "two-dimensional sphere" according to

$$R_1 = R/2, \tag{3.11}$$

("rule of Popov"), then we obtain the *exact* Herzian relationships for the contact radius and the normal force:

$$a = \sqrt{Rd}, \tag{3.12}$$

$$F_N(d) = \frac{4}{3} E^* \sqrt{Rd^3}. \tag{3.13}$$

In other words, the rule (3.11) means that the cross-section of the original three-dimensional profile (in our case, the sphere with the radius R) is stretched by a factor of 2 in the vertical direction.

In his dissertation from 2011, Heß [3] showed that a similar *exact* mapping is possible for an *arbitrary* axially-symmetric profile. In this chapter, we will apply the mapping rules determined by Heß without providing proof of their validity. A detailed derivation of these rules is provided in Chap. 17.

The focus of the following investigation is the contact between axially-symmetric bodies and an elastic half-space. Let the axis of symmetry be z and the surface of the elastic half-space be given by $z = 0$. We parameterize the surface of the half-space using the Cartesian coordinates x and y. Now, we consider an axially-symmetric body with the profile

$$\tilde{z} = f_n(r) = c_n r^n, \tag{3.14}$$

where $r = \sqrt{x^2 + y^2}$, C_n is a constant, and n represents an arbitrary positive number (not necessarily an integer). We now define a one-dimensional profile according to[4]

$$\tilde{z} = g_n(x) = \tilde{c}_n |x|^n. \tag{3.15}$$

As shown in Chap. 17, the contact between the three-dimensional profile (3.14) and the elastic half-space is equivalent to that of the two-dimensional profile (3.15) and the linearly elastic foundation (3.4) if the following *rule of Heß* is applied:

$$\tilde{c}_n = \kappa_n c_n, \quad \kappa_n = \frac{\sqrt{\pi}}{2} \frac{n\Gamma(\frac{n}{2})}{\Gamma(\frac{n}{2} + \frac{1}{2})}, \tag{3.16}$$

where $\Gamma(n)$ is the gamma function:

$$\Gamma(n) = \int_0^\infty t^{n-1} e^{-t} \mathrm{d}t. \tag{3.17}$$

[4] Let it be pointed out here that, as in the introductory examples, a one-dimensional profile is generally denoted with $g(x)$ and a three-dimensional profile with $f(r)$. Both are defined as being positive from the tip of the indenter upwards, which is additionally introduced as the coordinate $\tilde{z}$ (see Fig. 3.4).

The exact equivalence between the three-dimensional and one-dimensional problem is valid for the relationships between the normal force, the contact radius, and the indentation depth. In Table 3.1, the values of the scaling factor κ_n are presented for various values of n and in Fig. 3.3 for $0 < n \leq 5$, they are shown graphically.

Here, the values for a conical and a parabolic indenter are pointed out. The corresponding scaling factors are $\kappa_1 = \frac{1}{2}\pi$ and $\kappa_2 = 2$. The latter is, of course, consistent with the *rule of Popov*, which requires dividing the radius of curvature by 2.

The fact that it is possible to exactly map a three-dimensional contact problem to a one-dimensional linearly elastic foundation not only for profiles of the form (3.14), but rather *for arbitrary superpositions* of such forms is extremely important. We now consider a superposition of multiple profiles:

$$f(r) = \sum_{n=1}^{\infty} f_n(r) = \sum_{n=1}^{\infty} \mathrm{c}_n r^n. \tag{3.18}$$

In this case, the rule of Heß is applied as follows: From the profile (3.18), a one-dimensional profile is generated

$$f(r) = \sum_{n=1}^{\infty} c_n r^n \Rightarrow g(x) = \sum_{n=1}^{\infty} \tilde{c}_n |x|^n. \tag{3.19}$$

In Chap. 17, it is shown that by indenting the profile (3.19) into a linearly elastic foundation with a stiffness according to (3.4), the relationships between the normal force, contact radius, and the indentation depth remain the same as those in the three-dimensional case.

Table 3.1 Scaling factor κ_n for various exponents of the form function

n	0.5	1	2	3	4	5	6	7	8	9	10
κ_n	1.311	1.571	2	2.356	2.667	2.945	3.2	3.436	3.657	3.866	4.063

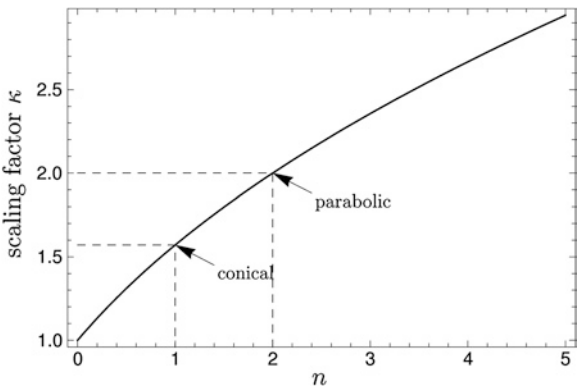

Fig. 3.3 Dependence of the scaling factor κ on the exponent n

The ability to map contacts between three-dimensional, axially-symmetric bodies of the form (3.14) to one-dimensional systems results from simple general scaling arguments and it is informative to discuss these briefly at this point. From dimensional analysis and self-affinity[5] of the profile (3.14), it arises that the contact radius and the indentation depth are related by the same exponential power n as $\tilde{z}$ and R:

$$d = \kappa_n c_n a^n, \tag{3.20}$$

where κ_n is a dimensionless constant. By pressing the one-dimensional profile (3.15) into the linearly elastic foundation, the indentation depth is trivially determined according to

$$d = \tilde{c}_n a^n. \tag{3.21}$$

By choosing a suitable $\tilde{c}_n = \kappa_n c_n$, one can always guarantee that the relationship between the indentation depth and the contact radius is correct in both cases. Furthermore, the differential contact stiffness is given in both the one-dimensional case as well as the three-dimensional case by

$$\frac{\partial F_N}{\partial d} = 2aE^* \tag{3.22}$$

(proof is given by Pharr et al. [4] or Popov [5]). By integrating this equation and taking (3.21) into consideration, the following relationship is obtained for both the one-dimensional and three-dimensional case:

$$F_N = \int \mathrm{d}F_N = 2E^* \int a\mathrm{d}(d) = 2E^* \int a\tilde{c}_n n a^{n-1}\mathrm{d}a = 2E^*\tilde{c}_n \frac{n}{n+1} a^{n+1}. \tag{3.23}$$

Inarguably, the force as a function of indentation depth must be the same in both cases:

$$F_N = \frac{2n}{n+1} E^* \tilde{c}_n^{-1/n} d^{\frac{n+1}{n}}. \tag{3.24}$$

If we constrain ourselves to the force–displacement relationship, then the ability to map three-dimensional systems to one-dimensional systems becomes even more general and is possible for arbitrary self-affine surfaces, regardless if they are axially-symmetric or not: The exponential dependence (3.24) is only contingent on the self-affinity and is valid for arbitrary surfaces with given Hurst exponents. Obviously, the correct coefficient can always be found by stretching the profile by the appropriate factor if the exponent in the force–displacement relationship is correct. As we will see in Chap. 10, this is also valid for self-affine, fractally rough surfaces. This paves the way for the fast calculation of contacts with rough surfaces and is, therefore, especially interesting.

Also, the superposition rule (3.19) has a simple physical meaning and requires only that the medium exhibits a linear behavior. Let us consider the two profiles

[5] For self-affinity, the following property is understood: If the profile (3.14) is stretched in the horizontal direction by the factor C and simultaneously in the vertical direction by a factor C^n, then one obtains the original profile. The exponent n is known as the *Hurst exponent*.

$f_1(r)$ and $f_2(r)$ being pressed into an elastic half-space. The first profile requires the indentation force $F_1(a)$ in order to obtain the contact radius a. The second profile, on the other hand, requires the force $F_2(a)$ in order to reach the *same contact radius a*. We denote the corresponding indentation depths with $d_1(a)$ and $d_2(a)$. If we initially consider the indention of $f_1(r)$ and then *additionally* apply $f_2(r)$ to the *same contact area,* with the radius a, then it directly follows from the linearity of the medium that the necessary force is

$$F_N(a) = F_1(a) + F_2(a). \tag{3.25}$$

The indentation depth, thereby, is

$$d(a) = d_1(a) + d_2(a). \tag{3.26}$$

These are exactly the two properties that are necessary for the mapping of superimposed profiles according to Eq. (3.19). In order to prevent confusion, we would like to stress that the principle of superposition is not valid (or is not exact) if the areas of application of both profiles are not the same.

3.3 General Mapping of Axially-Symmetric Profiles

The previous considerations dealt with the simplest mapping rules which are valid for contact profiles in the form of power functions. By choosing an arbitrary, positive real exponent and using the principle of superposition due to linearity, a large number of axially-symmetric contacts are able to be exactly mapped. The equivalence between one-dimensional and three-dimensional systems, however, is in no way restricted to such systems, but is generally valid for *all* axially-symmetric contacts with a simply connected contact area. The calculation of an equivalent profile using the profile function of the three-dimensional contact is conducted using the following formula:

$$g(x) = |x| \int_0^{|x|} \frac{f'(r)}{\sqrt{x^2 - r^2}} \mathrm{d}r, \tag{3.27}$$

the validity of which will be proven in Chap. 17. The fact that in the case of the power function (3.14), this rule leads to the simple scaling relation (3.16) is also explained here. Except for the explicit application of the formula (3.27), nothing changes in the procedure of the reduction method in order to determine the relationships between contact radius, indentation depth, and normal force. In the following, we would like to explain the procedure step by step using an example. For this, we consider the indentation of the following piecewise-defined profile into an elastic half-space:

$$f(r) = \begin{cases} 0 & \text{for } 0 \le r < b \\ \frac{r^2 - b^2}{2R} & \text{for } b \le r \le a \end{cases}. \tag{3.28}$$

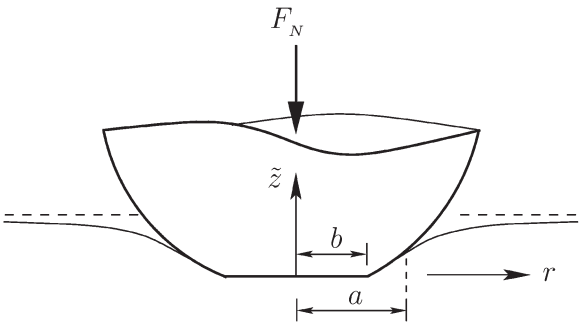

Fig. 3.4 Qualitative presentation of the indentation of a parabolic profile with a flattened tip into an elastic half-space

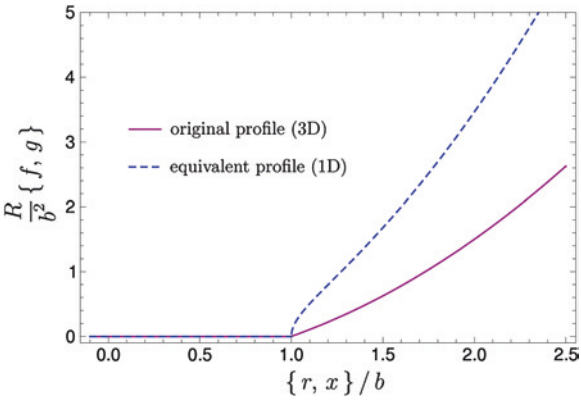

Fig. 3.5 Parabolic indenter with "worn" tip: comparison between original and equivalent profile

As can be gathered from Fig. 3.4, we can interpret the profile as an asperity which was originally parabolic, the tip of which, however, has been worn down through time.

The application of (3.27) requires the derivative of the original profile (3.28)

$$f'(r) = \begin{cases} 0 & \text{for } 0 \le r < b \\ \frac{r}{R} & \text{for } b \le r \le a \end{cases}, \tag{3.29}$$

which, after insertion into (3.27) and subsequent integration, leads to the equivalent one-dimensional profile[6]

$$g(x) = \begin{cases} 0 & \text{for } 0 \le |x| < b \\ \frac{|x|}{R}\sqrt{x^2 - b^2} & \text{for } b \le |x| \le a \end{cases}. \tag{3.30}$$

This profile is compared to the original in Fig. 3.5.

[6] Frequently, the one-dimensional profile is referred to in the following; this is to be understood, of course, as the profile in the one-dimensional model.

Naturally, the special case of $b = 0$ coincides with the mapping rule of Popov, of which one may be convinced by comparing (3.28) and (3.30) for this case.

For a known equivalent profile, we can now proceed to the solution of the contact problem using the aforementioned reduction process. In order to accomplish this, we must merely press the rigid profile described by (3.30) into the one-dimensional linearly elastic foundation, which results in a surface displacement of

$$u_z(x) = d - g(x) = d - \frac{|x|}{R}\sqrt{x^2 - b^2}. \tag{3.31}$$

The indentation depth, contact radius, and normal force must reveal the exact three-dimensional dependencies. The indentation depth as a function of contact radius results from requiring that the displacement at the edge of the contact approaches zero:

$$u_z(a) = 0 \quad \Rightarrow \quad d = g(a) = \frac{a}{R}\sqrt{a^2 - b^2}. \tag{3.32}$$

The normal force is the sum of the spring forces

$$F_N = E^* \int_{-a}^{a} \left[d - g(x)\right] \mathrm{d}x = 2E^* \int_{0}^{a} d \, \mathrm{d}x - \frac{2E^*}{R} \int_{b}^{a} x\sqrt{x^2 - b^2} \, \mathrm{d}x, \tag{3.33}$$

which provides

$$F_N(a) = \frac{2E^*}{3R}\left(2a^2 + b^2\right) \cdot \sqrt{a^2 - b^2}. \tag{3.34}$$

after integration and rearranging with the help of (3.32). The results (3.32) and (3.34) obtained by using the reduction method are exactly those derived by Ejike [6] for the three-dimensional problem. For the sake of completeness, let us state the relationship between normal force and indentation depth, which after solving (3.32) with respect to a and subsequently inserting this into (3.34), results in

$$F_N(d) = \frac{\sqrt{2}E^* b^3}{3R}\left(2 + \sqrt{1 + \left(\frac{2R}{b^2}d\right)^2}\right) \cdot \sqrt{-1 + \sqrt{1 + \left(\frac{2R}{b^2}d\right)^2}}. \tag{3.35}$$

Further contact problems that require the explicit application of formula (3.27) for the calculation of the equivalent profile can be found in the practice exercises at the end of this and the following two chapters.

3.4 The Mapping of Stress

In the one-dimensional contact problem with the linearly elastic foundation, the stresses are not able to be directly determined. Although the relationships between the force, displacement, and contact radius may be correctly obtained, it seems

as if the contact-mechanical information dealing with the stress is lost. In reality, however, this is not the case. In the aforementioned dissertation by Heß [3], it was shown that the stress distribution for an arbitrary three-dimensional contact is able to be reproduced for a corresponding one-dimensional problem. The required derivations can be found in Chap. 17. In the present chapter, we will explain the rules for the calculation without the necessary evidence.

For the linearly elastic foundation, the spring forces $f_N(x)$ are directly given for every contact configuration. The distributed load $q(x)$ (or linear force density) is also able to be directly defined:

$$q(x) = \frac{f_N(x)}{\Delta x}. \tag{3.36}$$

Among others properties, it will be shown in Chap. 17 that the normal stress $\sigma_{zz}(r)$ in the contact area of a three-dimensional contact problem may be found from the distributed load $q(x)$ using the following integral transformation (the Abel transformation):

$$\sigma_{zz}(r) = \frac{1}{\pi} \int_r^\infty \frac{q'(x)}{\sqrt{x^2 - r^2}} \mathrm{d}x. \tag{3.37}$$

As an example of the application of this procedure, we once again consider the Hertzian contact problem. For the distributed load, it follows from (3.9) that

$$\begin{aligned} q(x) &= E^* \left(d - \tfrac{x^2}{2R_1} \right), \quad \text{for} \quad |x| < a = \sqrt{2R_1 d}. \\ q(x) &= 0, \qquad\qquad\quad \text{for} \quad |x| > a = \sqrt{2R_1 d} \end{aligned} \tag{3.38}$$

The derivative is $q'(x) = -E^* x / R_1$ within the contact area and zero outside of it. Insertion into (3.37) leads to

$$\sigma_{zz}(r) = -\frac{E^*}{\pi R_1} \int_r^\infty \frac{x \mathrm{d}x}{\sqrt{x^2 - r^2}} = -\frac{E^*}{\pi R_1} \int_r^a \frac{x \mathrm{d}x}{\sqrt{x^2 - r^2}} = -\frac{2}{\pi} E^* \left(\frac{d}{R} \right)^{1/2} \sqrt{1 - \left(\frac{r}{a} \right)^2}, \tag{3.39}$$

which corresponds exactly with the known Herzian solution.

Further examples to the calculation of the stress in axially-symmetric contacts according to Eq. (3.37) will be considered in the exercises at the end of this chapter.

3.5 The Mapping of Non-Axially-Symmetric Bodies

The equation for contact stiffness written in the form

$$k_z = 2E^* \beta \sqrt{\frac{A}{\pi}} \tag{3.40}$$

is also valid for non-circular cross-sections (A is the contact area). The constant β is always on the order of magnitude of 1 for "simple" profiles (see [7]):

$$\begin{array}{ll} \text{circular cross-section:} & \beta = 1.000 \\ \text{triangular cross-section:} & \beta = 1.034 \\ \text{square cross-section:} & \beta = 1.012 \end{array} \tag{3.41}$$

Equation (3.40) can be written in the form (3.1), if we define the effective diameter D as

$$D = 2\beta\sqrt{\frac{A}{\pi}}. \tag{3.42}$$

This rule allows for non-axially symmetric contacts to be mapped to a one-dimensional contact with a linearly elastic foundation.

3.6 Problems

Problem 1 Solve the problem of the contact between a cone and an elastic half-space (Fig. 3.6a) using the reduction method. Calculate the contact radius and the normal force as a function of the indentation depth.

Solution The form of the cone is described by the equation $f(r) = \tan\theta \cdot r$. The corresponding scaling factor has the value $\kappa_1 = \pi/2$, so that the one-dimensional profile is given by $g(x) = (\pi/2)\tan\theta \cdot |x|$. If the indenter is pressed to a depth of d, then the vertical displacement of the foundation at point x is given by $u_z(x) = d - (\pi/2)\tan\theta \cdot |x|$. We calculate the contact radius by demanding that $u_z(a) = 0$ and in this way, obtain the desired dependence on the indentation depth:

$$a = \frac{2}{\pi}\frac{d}{\tan\theta}. \tag{3.43}$$

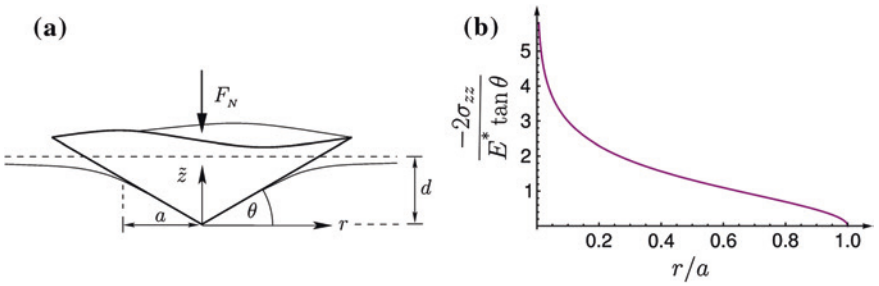

Fig. 3.6 (**a**) Contact between a rigid conical indenter and an elastic half-space. (**b**) Pressure distribution for the normal contact between a conical indenter and an elastic half-space

The normal force is obtained by "summing the spring forces":

$$F_N = 2E^* \int_0^a u_z(x)\mathrm{d}x = 2E^* \int_0^a (d - (\pi/2)\tan\theta \cdot x)\mathrm{d}x = \frac{2}{\pi} E^* \frac{d^2}{\tan\theta}. \quad (3.44)$$

Both results correspond *exactly*, of course, with those of the three-dimensional contact problem [8].

Problem 2 Let the profile $f(r) = C \cdot r^n$ be given for a rigid axially-symmetric indenter that is pressed into an elastic half-space. Determine the contact radius and the normal force in dependence on the indentation depth by using the reduction method.

Solution The equivalent one-dimensional profile is $g(x) = C\kappa_n |x|^n$. The contact radius is calculated from the condition $g(a) = d$ as

$$a = \left(\frac{d}{C\kappa_n}\right)^{1/n}. \quad (3.45)$$

The displacement field is determined by $u_z(x) = d - C\kappa_n |x|^n$ and for the normal force, we obtain

$$F_N = 2E^* \int_0^a u_z(x)\mathrm{d}x = 2E^* \int_0^a \left(d - C\kappa_n x^n\right)\mathrm{d}x = \frac{2n}{n+1} \frac{E^* d^{\frac{n+1}{n}}}{(C\kappa_n)^{1/n}}. \quad (3.46)$$

Once again, the results provide the *exact* dependencies of the three-dimensional problem (see Chap. 17).

Problem 3 Analyze the contact between a half-space and a superimposed profile of the form $f(r) = \frac{r^2}{2R} + |r| \tan\theta$ using the reduction method. Determine the contact radius and the normal force with respect to indentation depth.

Solution The equivalent one-dimensional profile is

$$g(x) = \kappa_2 \frac{x^2}{2R} + \kappa_1 |x| \tan\theta = \frac{x^2}{R} + \frac{\pi}{2} |x| \tan\theta. \quad (3.47)$$

The contact radius is determined using the condition

$$g(a) = \frac{a^2}{R} + \frac{\pi}{2} a \tan\theta = d, \quad (3.48)$$

so that the following relationship between the contact radius and displacement results:

$$a = \sqrt{\left(\frac{\pi}{4} R \tan\theta\right)^2 + Rd} - \frac{\pi}{4} R \tan\theta. \quad (3.49)$$

The one-dimensional displacement field is given by $u_z(x) = d - \frac{x^2}{R} - \frac{\pi}{2}|x| \tan\theta$, where we obtain the equation

$$F_N = 2E^* \int_0^a u_z(x)\mathrm{d}x = 2E^* \int_0^a \left(d - \frac{x^2}{R} - \frac{\pi}{2}|x| \tan\theta\right)\mathrm{d}x \tag{3.50}$$

for the normal force, which leads to the following equation after integration:

$$F_N = 2E^* \left(da - \frac{a^3}{3R} - \frac{\pi}{4}a^2 \tan\theta\right). \tag{3.51}$$

Insertion of (3.49) and simple rearrangement with respect to the desired relationship between normal force and indentation depth leads to

$$\begin{aligned} F_N = \frac{\pi^3 R^2 (\tan\theta)^3 E^*}{96} &\left(\sqrt{1 + \frac{16d}{\pi^2 R(\tan\theta)^2}} - 1\right) \\ &\left(1 + \frac{32d}{R\pi^2(\tan\theta)^2} - \sqrt{1 + \frac{16d}{\pi^2 R(\tan\theta)^2}}\right). \end{aligned} \tag{3.52}$$

Problem 4 Calculate the stress distribution between a flat cylindrical indenter and an elastic half-space with the help of the Abel transformation.

Solution We begin by calculating the distributed load in the one-dimensional case. For a flat cylindrical indenter, the distributed load is constant and equal to

$$q(x) = \begin{cases} F_N/(2a), & \text{for } |x| < a \\ 0, & \text{for } |x| > a \end{cases}. \tag{3.53}$$

We obtain the derivative

$$q'(x) = \frac{F_N}{2a}(\delta(x + a) - \delta(x - a)), \tag{3.54}$$

where $\delta(x)$ denotes the Dirac delta function. The integral (3.37) takes the form

$$\sigma_{zz}(r) = \frac{1}{\pi} \int_r^\infty \frac{q'(x)}{\sqrt{x^2 - r^2}}\mathrm{d}x = \frac{1}{\pi}\frac{F_N}{2a} \int_r^\infty \frac{(\delta(x + a) - \delta(x - a))}{\sqrt{x^2 - r^2}}\mathrm{d}x. \tag{3.55}$$

For the Dirac delta function equation $\int f(x)\delta(x - a)\mathrm{d}x = f(a)$ is valid if the integration area contains the point $x = a$ and is otherwise zero. Thus, the integration in (3.55) results in

$$\sigma_{zz}(r) = \frac{1}{\pi}\frac{F_N}{2a} = \begin{cases} -\frac{1}{\sqrt{a^2 - r^2}}, & \text{for } |r| < a \\ 0, & \text{for } |r| > a \end{cases}. \tag{3.56}$$

This is the *exact* stress distribution that exists in the three-dimensional contact between a rigid flat cylindrical indenter and an elastic half-space [1].

Problem 5 Calculate the stress distribution in a contact between a rigid cone and an elastic half-space with the help of the Abel transformation.

Solution We consider the equivalent one-dimensional model from Problem 1. The vertical displacement of the foundation at the point x is $u_z(x) = d - (\pi/2)\tan\theta \cdot |x|$, from which we obtain the distributed load $q(x) = E^* \cdot u_z(x) = E^*(d - (\pi/2)\tan\theta \cdot |x|)$. In order to calculate the normal stress, we insert the derivative $q'(x) = -(\pi/2)E^*\tan\theta \cdot \text{sign}(x)$ into Eq. (3.37)

$$\sigma_{zz}(r) = \frac{1}{\pi}\int_r^\infty \frac{q'(x)}{\sqrt{x^2 - r^2}}\mathrm{d}x = -\frac{1}{2}E^*\tan\theta \int_r^a \frac{\mathrm{d}x}{\sqrt{x^2 - r^2}}. \tag{3.57}$$

Taking the integral results in

$$\sigma_{zz}(r) = \begin{cases} -\frac{1}{2}E^*\tan\theta \cdot \ln\left(\frac{a}{r} + \sqrt{\left(\frac{a}{r}\right)^2 - 1}\right), & \text{for } r < a \\ 0, & \text{for } r > a \end{cases}, \tag{3.58}$$

which is, of course, also in this case the *exact* three-dimensional stress distribution. This is shown graphically in Fig. 3.6b.

Problem 6 Determine the normal force and normal stress for the contact between a rigid cylindrical indenter and a concave, parabolic profile (see Fig. 3.7) with the help of the reduction method. Instead of using the indentation depth d, the displacement should be formulated based on the geometric values of d_o and h. It is assumed that a complete contact is present.

Solution First, we define the surface displacement within the contact area for the axially-symmetric contact. For this, we use the average displacement d_o in place of

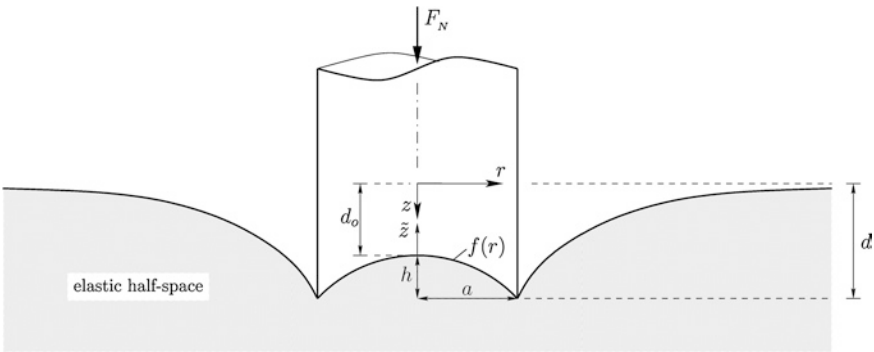

Fig. 3.7 Qualitative presentation of a (complete) indentation of a rigid cylindrical indenter with a concave, parabolic profile into an elastic half-space

the indentation depth d, so that $f(0) = 0$ is guaranteed for the concave profile in the same way as for the convex profile. Then, the following is valid:

$$u_z(r) = d_o - f(r) = d_o + \frac{h}{a^2} r^2. \tag{3.59}$$

The original profile contains a quadratic term, which we must simply multiply with the corresponding scaling factor in order to arrive at the geometry of the equivalent system:

$$g(x) = \kappa_2 f(|x|) = -2\frac{h}{a^2} x^2. \tag{3.60}$$

From the corresponding surface displacement in the one-dimensional model, we obtain a normal force of

$$F_N = 2E^* \int_0^a \left[d_o - g(x)\right] \mathrm{d}x = 2E^* \int_0^a \left(d_o + 2\frac{h}{a^2} x^2\right) \mathrm{d}x = 2E^* a \left(d_o + \frac{2}{3} h\right). \tag{3.61}$$

In order to calculate the normal stress in the original contact, we require the derivative of the distributed load $q'(x)$ in the reduced dimensions as well as the boundary condition $q(a)$:

$$q(x) = E^* \left(d_o + 2\frac{h}{a^2} x^2\right) \quad \Rightarrow \quad q'(x) = 4E^* \frac{h}{a^2} x \text{ and } q(a) = E^*(d_o + 2h). \tag{3.62}$$

Insertion of (3.62) into (3.37) leads to the desired normal stresses after integration and elementary rearrangement:

$$\sigma_{zz}(r) = -\frac{E^*}{\pi} \cdot \frac{d_o - 2h + 4h\left(\frac{r}{a}\right)^2}{\sqrt{a^2 - r^2}}. \tag{3.63}$$

Naturally, the results (3.61) and (3.63) correspond exactly to those of the three-dimensional, axially-symmetric contact, which is confirmed by comparison with the results given by Barber [9], if one takes into account the conversion $d_o = d - h$. Let it be once again insistently pointed out that a complete contact is assumed, which must satisfy the requirement of $\sigma_{zz}(0) \leq 0$. Then, from Eq. (3.63), the condition $d_o \geq 2h$ follows. Due to the fact that the reduction method in the form shown here is only suitable for the mapping of complete contacts (and not ring-shaped contact areas), this condition does not follow directly from the one-dimensional model. Furthermore, the exact mapping is only guaranteed for $F_N(d_o)$ and not for $F_N(d)$, because the maximum displacement (indentation depth) for concave profiles occurs on the boundary and not in the middle.

Problem 7 Formulate the method of dimensionality reduction for a transversally-isotropic medium.

Solution A transversally-isotropic medium is a medium that is isotropic in one plane. For crystalline bodies, this includes bodies in the hexagonal class of

crystals. Also, a fiber composite with all fibers oriented in parallel is a transversally-isotropic medium. A linearly transversally-isotropic medium can be completely defined by 5 elastic moduli. If we denote the axis of symmetry to be "3," then the axes "1" and "2" are "equivalent" and can be chosen arbitrarily within the plane which they define. Hooke's law for such a medium is as follows:

$$\begin{aligned}
\sigma_{11} &= C_{11}\varepsilon_{11} + C_{12}\varepsilon_{22} + C_{13}\varepsilon_{33} \\
\sigma_{22} &= C_{12}\varepsilon_{11} + C_{11}\varepsilon_{22} + C_{13}\varepsilon_{33} \\
\sigma_{33} &= C_{13}(\varepsilon_{11} + \varepsilon_{22}) + C_{33}\varepsilon_{33} \\
\sigma_{12} &= (C_{11} - C_{12})\varepsilon_{12} \\
\sigma_{23} &= 2C_{44}\varepsilon_{23} \\
\sigma_{31} &= 2C_{44}\varepsilon_{31}\,.
\end{aligned} \tag{3.64}$$

The applicability of the method of dimensionality reduction is based solely on the fact that the differential stiffness of a medium is determined exclusively by the current contact area. For axially-symmetric profiles, it is given by the stiffness of the contact between a flat, rigid cylindrical indenter and the elastic half-space. Therefore, the rule for the application of the method of dimensional reduction to an arbitrary linearly elastic medium is as follows: First, the stiffness k_z of the contact with a flat cylindrical indenter with the diameter D and the equivalent one-dimensional system as a linearly elastic foundation with a stiffness per unit length of k_z/D are determined. This method can be applied to any medium for which a solution with a rigid cylinder is known.

The solution for the stiffness of a contact between a flat, cylindrical indenter and a transversally-isotropic medium (with an axis of symmetry parallel to the normal vector) can be directly taken from the work of Yu [10]. It is given by Eq. (3.1) with

$$E^* = \frac{2\left(\bar{C}_{13}^2 - C_{13}^2\right)}{\bar{C}_{13}(\nu_1 + \nu_2)}, \tag{3.65}$$

where the following relationships are introduced:

$$\nu_1 = \left[\frac{\left(\bar{C}_{13} - C_{13}\right)\left(2\bar{C}_{13} - I_0\right)}{4C_{33}C_{44}}\right]^{1/2} + \left[\frac{\left(\bar{C}_{13} + C_{13}\right)I_0}{4C_{33}C_{44}}\right]^{1/2} \tag{3.66}$$

$$\nu_2 = \left[\frac{\left(\bar{C}_{13} - C_{13}\right)\left(2\bar{C}_{13} - I_0\right)}{4C_{33}C_{44}}\right]^{1/2} - \left[\frac{\left(\bar{C}_{13} + C_{13}\right)I_0}{4C_{33}C_{44}}\right]^{1/2} \tag{3.67}$$

$$\bar{C}_{13} = (C_{11}C_{33})^{1/2} \tag{3.68}$$

$$I_0 = \bar{C}_{13} - C_{13} - 2C_{44}. \tag{3.69}$$

Insertion of (3.66)–(3.69) into (3.65) results in

$$E^* = \frac{2\sqrt{C_{44}}\left(C_{11}C_{33} - C_{13}^2\right)}{\sqrt{C_{11}}\sqrt{\left(\sqrt{C_{11}C_{33}} - C_{13}\right)\left(C_{13} + 2C_{44} + \sqrt{C_{11}C_{33}}\right)}}. \tag{3.70}$$

Problem 8 Determine the indentation depth and the normal force as a function of contact radius for the normal contact between a sphere of radius R and a linearly elastic half-space with the help of the reduction method. Contrary to the parabolic approximation of Hertz, here the exact spherical form should be taken into account and the equivalent profile should be calculated with the general Eq. (3.27).

Solution The exact profile of a sphere with a radius of R is given by the function

$$f(r) = R - \sqrt{R^2 - r^2}. \tag{3.71}$$

The first derivative of (3.71) is

$$f'(r) = \frac{r}{\sqrt{R^2 - r^2}}. \tag{3.72}$$

Inserting (3.72) into the general formula (3.27) leads to the equation

$$g(x) = x \int_0^x \frac{r}{\sqrt{R^2 - r^2} \cdot \sqrt{x^2 - r^2}} \mathrm{d}r = -x \int_{z(0)}^0 \frac{\mathrm{d}z}{\sqrt{1 + z^2}}, \tag{3.73}$$

for which the elementary integral on the right results by using the substitution $z(r) = \dfrac{\sqrt{x^2 - r^2}}{\sqrt{R^2 - x^2}}$. The equivalent profile is

$$g(x) = x \cdot \operatorname{arsinh}\left(\frac{x}{\sqrt{R^2 - x^2}}\right) = \frac{1}{2} x \ln\left(\frac{R + x}{R - x}\right). \tag{3.74}$$

Figure 3.8 shows both of the "equivalent" profiles as well as their parabolic approximations. The dashed lines confirm the rule of Popov.

Simultaneously, the surface displacement of the linearly elastic foundation may be found with (3.74), which must tend to zero at the contact boundary and in this way, determines the indentation depth:

$$u_z(a) = 0 \quad \Rightarrow \quad d = g(a) = \frac{1}{2} a \ln\left(\frac{R + a}{R - a}\right). \tag{3.75}$$

The spring forces, which are proportional to the surface displacement, must be in equilibrium with the normal force

$$F_N = E^* \int_{-a}^{a} \left[d - g(x)\right] \mathrm{d}x = 2E^* da - E^* \int_0^a x \ln\left(\frac{R + x}{R - x}\right) \mathrm{d}x. \tag{3.76}$$

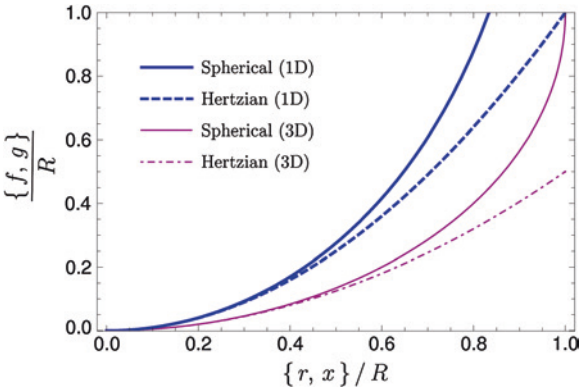

Fig. 3.8 Exact spherical form and parabolic approximation (Hertz) including the one-dimensional equivalents

A suitable partial integration initially provides

$$F_N = 2E^* a\left[d - \frac{R}{2} + \frac{R^2 - a^2}{4a}\ln\left(\frac{R+a}{R-a}\right)\right] \tag{3.77}$$

and after insertion of (3.75), the contact force is finally obtained as a function of contact radius:

$$F_N(a) = E^*\frac{R^2 + a^2}{2}\ln\left(\frac{R+a}{R-a}\right) - E^* Ra. \tag{3.78}$$

The indentation depth from (3.75) and the normal force from (3.78) correspond exactly to the three-dimensional contacts based on the solutions of Segedin [11], which are obtained using the Area-functions. Finally, let it be known that we could have just as well developed the spherical profile as a series. After multiplying the individual terms with the corresponding scaling factor, according to the rules of Heß, the equivalent profile (3.74) would have been given in the form of a power series. If the integral for the general formula (3.27) is not known, we have, in fact, no choice but to use this strategy.

References

1. K.L. Johnson, *Contact Mechanics*, Nachdruck der 1. Auflage (s.l.: Cambridge University Press, Cambridge, 2001), p. 6
2. V.L. Popov, S.G. Psakhie, Numerical simulation methods in tribology. Tribol. Int. **40**(6), 916–923 (2007)
3. M. Heß, *Über die exakte Abbildung ausgewählter dreidimensionaler Kontakte auf Systeme mit niedrigerer räumlicher Dimension* (Cuvillier, Berlin, 2011)
4. G.M. Pharr, W.C. Oliver, F.R. Brotzen, On the generality of the relationship among contact stiffness, contact area, and elastic modulus during indentation. J. Mater. Res. **7**(3), 613–617 (1992)

5. V.L. Popov, Contact Mechanics and Friction. Physical Principles and Applications (Springer, Berlin Heidelberg 2010), pp. 69–70.
6. U.B.C.O. Ejike, The stress on an elastic half-space due to sectionally smooth-ended punch. J. Elast. **11**(4), 395–402 (1981)
7. R.B. King, Elastic analysis of some punch problems for a layered medium. Int. J. Solids Struct. **23**(12), 1657–1664 (1987)
8. A.E.H. Love, Boussinesq's problem for a rigid cone. Q. J. Math. **10**, 161–175 (1939)
9. J.R. Barber, Indentation of the semi-infinite elastic solid by a concave rigid punch. J. Elast. **6**(2), 149–159 (1976)
10. H.Y.A. Yu, Concise treatment of indentation problems in transversely isotropic half-spaces. Int. J. Solids Struct. **38**(10), 2213–2232 (2001)
11. C.M. Segedin, The relation between load and penetration for a spherical punch. Mathematika **4**, 156–161 (1957)

Chapter 4
Normal Contact with Adhesion

Markus Heß and Valentin L. Popov

4.1 Introduction

The miniaturization of components and the manufacturing of ever smoother surfaces are a mark of the constant improvements in micro and nano-technologies today. For the length scales associated herewith, the adhesion forces must be doubtlessly taken into account. However, adhesion is also important for contacts in which one partner is composed of a very soft material. Above all, the adhesion between rough surfaces is a central research topic in this respect, as it deals with the friction of rubbers and the contact between biological structures.

From a theoretical point of view, one can name two main ansätze which were developed in order to describe adhesive contacts for *elastic*, parabolic bodies. The first is the theory of Johnson et al. [1] (JKR theory), which takes adhesion forces within the contact area into account. In this case, the contact radius in the equilibrium state is calculated from the minimum in the total energy, which in turn, is obtained from the elastic deformation energy, the potential of external forces, and the surface energy of the contacting bodies. On the other hand, in the theory developed by Derjagin et al. [2] (DMT theory), the molecular forces of attraction act only within a ring outside of the contact area. They naturally contribute to the normal force, however, it is assumed that they cause no deformation. Within the framework of DMT theory, the maximum magnitude of the adhesion force corresponds to that which Bradley derived in 1932 [3] for the adhesive contact between rigid spheres. Because the JKR theory diverges from the DMT theory, it appears at first that the two theories contradict each other. Tabor [4] was able to successfully explain this discrepancy by investigating the areas of validity of both theories in greater detail and defining them based on a dimensionless parameter. According to his findings, DMT theory is suitable for describing the contact of small, rigid spheres, while JKR theory is more adept at describing large, soft spheres. Johnson and Greenwood [5] created a map of adhesion, which graphically depicts the areas

V.L. Popov and M. Heß, *Method of Dimensionality Reduction in Contact Mechanics and Friction*, DOI 10.1007/978-3-642-53876-6_4

of validity for various adhesion theories. Furthermore, they pointed out the fact that the JKR theory still provides good results outside of its actual area of validity. It is possible that this is the reason that the JKR theory is primarily used to describe adhesion.

In this chapter, we will discuss how the leading adhesion theory from Johnson, Kendall, and Roberts is able to be exactly mapped using the method of dimensionality reduction. To begin, we will concentrate on a pure formulation of the simple rules of application for the adhesive normal contact and refrain from presenting the required evidence. Subsequently, these rules will be explained in more detail, which requires a certain understanding of the theoretical background on the adhesion in three-dimensional contacts, which we will also provide. For those not satisfied with these short explanations, the entirety of the necessary evidence may be found in Chap. 17.

4.2 Rule of Heß for the Adhesive Contact Between Axially-Symmetric Bodies

Adhesive contacts of axially-symmetric bodies can also be exactly mapped to a one-dimensional equivalent model. The rule for this mapping was developed by one of the authors (Heß) [6]. It is based on the basic idea of Johnson, Kendall, and Roberts that *the contact with adhesion arises from the contact without adhesion plus a rigid-body translation*. Because both parts of the contact problem can be mapped to a one-dimensional equivalent model with a modified geometry, then this is true of the entire problem. The rule of Heß is as follows: If an indenter with the modified form described in Chap. 3 is initially pressed into a linearly elastic foundation and then pulled out, as shown in Fig. 4.1, then the springs on the edge of the profile will detach upon reaching a critical length

$$\Delta\ell_{\max}(a) = \sqrt{\frac{2\pi a\,\Delta\gamma}{E^*}}, \tag{4.1}$$

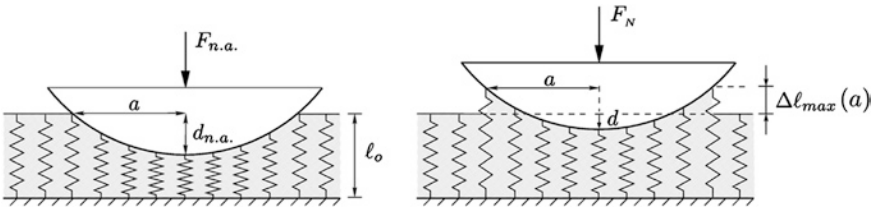

Fig. 4.1 Qualitative presentation of the indentation and separation process for the reduction method. The model shown exactly maps the adhesive contact of parabolic bodies and therefore, exactly mirrors JKR theory

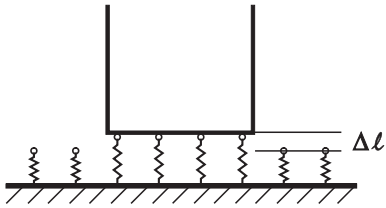

Fig. 4.2 Equivalent one-dimensional system for the adhesive contact between a flat, cylindrical indenter and an elastic half-space

where $\Delta\gamma$ is the separation energy of the bodies per unit area, which will be explained later in more detail. Here, it is worth noting that the separation criterion is not local, due to its dependence on the changing contact radius.

In order to illustrate the simple application of this rule, we will consider the adhesive contact between a flat, cylindrical indenter with the radius a and an elastic half-space (Fig. 4.2).

In this case, all springs will simultaneously detach as soon as the critical length (4.1) is reached. The total normal force required to separate the indenter from the substrate is then

$$F_A = 2E^* a\sqrt{\frac{2\pi a\,\Delta\gamma}{E^*}} = \sqrt{8\pi a^3 E^* \Delta\gamma}, \tag{4.2}$$

which corresponds exactly to the three-dimensional result [7]. For the problems at the end of this chapter, we will consider this type of contact problem once again by supplementing the general structure with relevant alterations. There, as well as in Sects. 4.4 and 4.5, there are numerous examples provided. However, before we proceed with these examples, we would like to explain the theoretical considerations that lead to Rule (4.1) in more detail. This is done primarily in Sect. 4.4, which contains further simple rules which help to determine the normal stress and the stability of the system. In this way, critical quantities can be determined very simply. We begin the theoretical consideration with the compatibility of the JKR theory with the ansätze from linear fracture mechanics. Those only interested in the practical application of the method of dimensionality reduction to adhesive contacts may continue directly with Sect. 4.4.

4.3 The Adhesive Contact and Griffith Crack

In the theory of Johnson, Kendall, and Roberts, the contact radius of an adhesive contact arises from the minimum total energy, which consists of the elastic deformation energy U_E, the potential of external forces U_P, and the surface energy U_S. In the original publication [1], it was already indicated that this energy ansatz is the same as that of Griffith [8, 9], which was once used to investigate fractures in

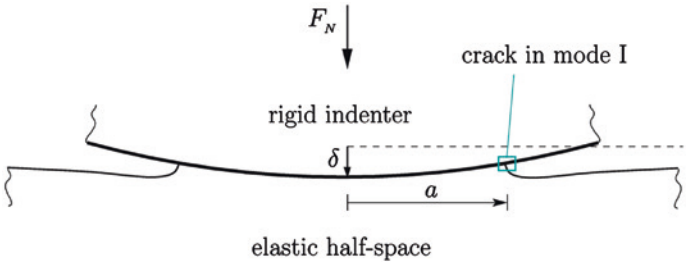

Fig. 4.3 Qualitative presentation of an adhesive contact between a rigid, curved body and an elastic half-space; the boundary of the contact can be referred to as the crack tip

brittle material[1] and is nothing more than the first law of thermodynamics. Maugis et al. [10, 11] conducted more penetrating thermodynamic considerations and proved, among other things, the compatibility of the JKR theory with that of linearly elastic fracture mechanics. The free boundary of the adhesive contact may, therefore, be referred to as a mode I crack,[2] which propagates either inwards or outwards based on changes in the contact surface. The decisive steps for the energy ansatz are very quickly explained. For this, we consider the adhesive contact between a rigid, curved body and an elastic half-space, according to Fig. 4.3. The indenter is loaded by an external force of F_N and, with the half-space, forms a contact area with a radius of a; in order to avoid confusion with differentials, the indentation depth will be denoted by δ in this section.

Initially, we assume that the indentation depth δ and the contact area A which describe the equilibrium state of the system are extensive properties. According to the first law of thermodynamics, a contribution of work from the external load, causes a change in the sum of the elastic deformation energy U_E and the surface energy U_S:

$$\mathrm{d}U_E(A,\delta) + \mathrm{d}U_S(A) = F_N(A,\delta)\mathrm{d}\delta. \tag{4.3}$$

The surface energy is not dependent on the indentation depth and is given by

$$U_S(A) = -\Delta\gamma \cdot A. \tag{4.4}$$

Here, $\Delta\gamma$ is the work that must be done per unit area against interatomic forces in order to separate the two solids, which is also known under the name of the Dupré energy of adhesion. It is dependent on the (specific) surface energies γ_1 and γ_2 of both bodies as well as the energy of the interface γ_{12}:

$$\Delta\gamma := \gamma_1 + \gamma_2 - \gamma_{12} \tag{4.5}$$

[1] More specifically, Griffith investigated the stability of a crack in the middle of a disc loaded in tension.

[2] The opening mode (mode I crack) is the separation mode for which the tensile stress acts *perpendicular* to the plane of the crack.

and can be interpreted as the "effective" interface energy. Insertion of (4.4) into (4.3) results in

$$\mathrm{d}U_E(A,\delta) - \Delta\gamma \cdot \mathrm{d}A = F_N(A,\delta)\ \mathrm{d}\delta. \tag{4.6}$$

By means of the Legèndre transformation, we can switch the independent extensive variables δ and F_N. In this way, we obtain

$$-\mathrm{d}U_E^K(A,F_N) - \Delta\gamma \cdot \mathrm{d}A = -\delta(A,F_N)\ \mathrm{d}F_N \quad \text{with} \quad U_E^K := F_N\delta - U_E, \tag{4.7}$$

in which U_E^K stands for the complementary elastic energy. By separating the total derivatives with respect to the corresponding variables, we obtain the laws of Castigliano and Engesser:

$$\left(\frac{\partial U_E}{\partial \delta}\right)_A = F_N \ \text{ or } \ \left(\frac{\partial U_E^K}{\partial F_N}\right)_A = \delta\,. \tag{4.8}$$

Furthermore, we now have two different possibilities for calculating the elastic energy release rate $\mathcal{G}$:

$$\mathcal{G} := \left(\frac{\partial U_E}{\partial A}\right)_\delta = -\left(\frac{\partial U_E^K}{\partial A}\right)_{F_N}. \tag{4.9}$$

In equilibrium, the mechanical energy released by a decrease in contact area must correspond to the energy required to form the new surface:

$$\mathcal{G} = \Delta\gamma =: \mathcal{G}_c. \tag{4.10}$$

Equation (4.10) once again provides the energetic fracture criterion of Griffith. Here, the effective interface energy $\Delta\gamma$ can be interpreted as the critical energy release rate $\mathcal{G}_c$ at which quasi-static fracture progression begins. The difference $\mathcal{G} - \Delta\gamma$ is occasionally called the *driving force* (with the units of linear force density) for the tip of the fracture and allows for the kinetic adhesive process to be investigated.

The energetic fracture criterion from Griffith in the form of (4.10) contains the energy release rate as a parameter and, as a result, is seen as a *global* fracture criterion. An equivalent criterion, and for our purposes more appropriate due to its *local* characteristic, is found using the concept of stress intensity. Irwin [12] recognized the fundamental fact that the singularities of all stress fields for all fracture types are similar in the fracture near field, and therefore, used their intensities for the investigation of fracture mechanics. The ligament stresses and the displacements which exist, for example, in the near field of the fracture shown in Fig. 4.4 with the separation mode I are

$$\sigma_{zz}(\eta,\beta=0) = \frac{K_I}{\sqrt{2\pi\eta}} \ \text{ and } \ u_z(\eta,\beta=\pm\pi) = \pm\frac{2}{E^*}K_I\sqrt{\frac{\eta}{2\pi}}\,. \tag{4.11}$$

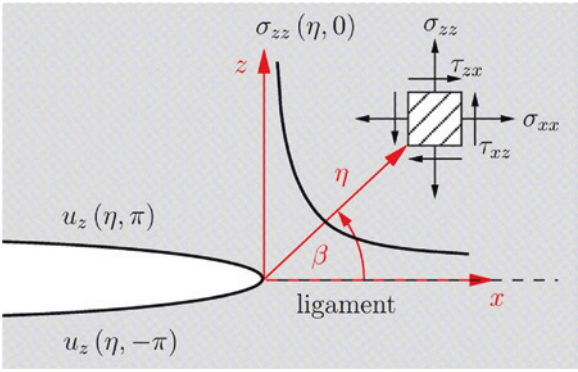

Fig. 4.4 Qualitative presentation of the ligament stress and the opening form of a mode I crack

The stress intensity factor K_I, which is dependent on the material as well as the geometry, length, and loading of the fracture, can be obtained if the ligament stress is known:

$$K_I := \lim_{\eta \to 0} \sqrt{2\pi\eta}\, \sigma_{zz}(\eta, 0). \tag{4.12}$$

According to Irwin, fracture propagation occurs only after K_I reaches the so-called fracture toughness K_{Ic} of the material, which must, in turn, be determined experimentally on standardized fracture experiments. Therefore, the *local* fracture criterion from Irwin for a mode I crack is

$$K_I = K_{Ic}. \tag{4.13}$$

Of course, no real material can withstand the (theoretically) infinitely large stress. Except for very brittle materials, a relaxation in stress occurs in the area near the fracture tip due to inelastic deformation. Furthermore, regardless of the material, a small zone always exists in which non-linear microscopic processes occur. As long as the combination of the plastic and microscopic zones is much smaller than the zone in which K_I dominates, the elastic near field will control the processes occurring in this field, allowing the use of the concept of stress intensity. The fact that the K concept and the fracture criterion from Griffith are equivalent was proven by Irwin for which he calculated the work required to close a fracture of length Δa[3]:

$$\mathcal{G} = \frac{K_I^2}{2E^*}. \tag{4.14}$$

Equation (4.14) is for a mode I crack. If a combined fracture load is present for which all three separation modes occur, then the individual energy release rates

[3] The equation is based on a fracture in a planar state of deformation; we may assume that locally in an axially-symmetric contact with adhesion, every point on the contact boundary exhibits this state.

must be summed. In the case of a fracture interface between two elastically similar materials, the following is then valid:

$$\mathcal{G} = \frac{1}{2E^*}\left(K_I^2 + K_{II}^2\right) + \frac{1}{4}\left(\frac{1}{G_1} + \frac{1}{G_2}\right)K_{III}^2. \tag{4.15}$$

With the help of this generalized presentation, the interaction between adhesion and friction can be determined [13].

It may have been the equivalence of the concepts of the fracture mechanism that motivated Maugis and Barquins [14, 15] to use Sneddons theory [16] for the mapping of adhesive contacts; the analogy between JKR theory and the Griffith theory of fracture mechanics was already proven at this time. Thus, the concept of the stress intensity factor must also exist in Sneddons theory. The original equations from Sneddon contain a (still arbitrary) rigid body translation, which is responsible for a singularity in the stress at the contact boundary. The translation is that which results from pressing a flat cylindrical indenter into a half-space and corresponds to that of the initial approximation for a mode I crack. Furthermore, the difference in the normal displacement between the indenter and surface of the half-space outside of the contact area is the same as the shape of the fracture in Eq. (4.11), so that a connection exists between the rigid body degree of freedom and the intensity factor. For contacts without adhesion, with the assumption that the profile is convex, the Boussinesq condition must be met, meaning that the singularity at the contact boundary disappears. The only difference between the two theories is the rigid body translation. This causes a tensile stress for which the distribution is the same as that under a flat cylindrical indenter. This is an essential relationship, which we would like to stress:

> *The contact with adhesion results from the contact without adhesion plus a rigid body translation.*

Even the original theory of Johnson, Kendall, and Roberts touches on this principle, which extends the Hertzian contact by adding adhesion. This theory was discussed in a generalized form at the beginning of this chapter. It requires, among other things, that the energy of the elastic deformation be known, which in turn, can be determined in two parts. One of these comes from the non-adhesive indentation process, while the other results from the decompression at a constant contact area. Figure 4.5 explains the superposition of the two loading cases. The indentation process with a force $F_{n.a.}$ occurs without adhesion, so that the resulting stresses and surface displacements are for a Hertzian contact. Due to the successive increase in the relative interface energy, the subsequent unloading from $F_{n.a.}$ to F_N occurs for a constant contact area. Because of this, all points in the contact area must undergo a constant displacement. Therefore, the unloading is the same as for the contact with a flat indenter, the characteristic stress distribution for which is responsible for the infinitely large tensile stress at the contact boundary.

This singularity can be seen in Fig. 4.5b, the stresses for which are shown with respect to their mean in the non-adhesive contact. Interestingly, Johnson [17] had already recognized the ability to use superposition to describe a contact with adhesion in 1958. The non-physical excess in stress on the boundary, however, led him

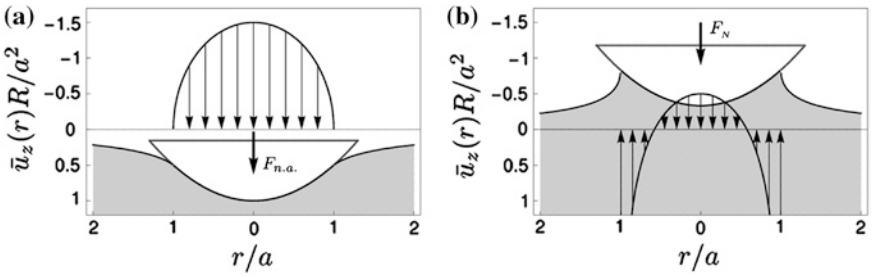

Fig. 4.5 **a** Hertzian spherical contact caused by the normal force $F_{n.a.}$, which leads to the same contact radius as in the adhesive case under the load of F_N; **b** Equilibrium state of the adhesive contact; more exactly, the critical state under a *fixed-load* condition is actually shown here

to *rule out* adhesion, which was in accord with the experimental works of Bowden and Tabor at the time.

4.4 Full Reduction of the Adhesive, Elastic Contact

The central notion of the exact mapping of axially-symmetric contacts with adhesion is the superposition concept described in the last section. According to this, the contact without adhesion must merely be superimposed with a rigid body translation. This means that the normal stress distribution in the contact area is

$$\sigma_{zz}(r) = \sigma_{n.a.}(r) + \frac{\Delta F}{2\pi a\sqrt{a^2 - r^2}} \quad \text{with} \quad \Delta F := F_{n.a.} - F_N = 2E^* a(d_{n.a.} - d), \tag{4.16}$$

where the second term is the stress distribution under a flat indenter described by Boussinesq. Remember that the values with the index "n.a." are those for a contact without adhesion for which the same contact radius is reached as that in a contact with adhesion. They belong to the (fictitious) indentation process for the JKR theory, which was shown in Fig. 4.5a. The stress intensity factor for the distribution in (4.16) can be easily calculated using Eq. (4.12):

$$K_I(a) = \frac{\Delta F}{2a\sqrt{\pi a}}. \tag{4.17}$$

By taking into consideration the fact that the concepts of Griffith and Irwin (4.14) are equivalent and that the equilibrium condition (4.10) is met, then

$$\Delta F = \sqrt{8\pi E^* a^3 \Delta\gamma}, \tag{4.18}$$

with which the indentation depth and the normal force can be directly determined for the adhesive case:

$$d(a) = d_{n.a.}(a) - \sqrt{\frac{2\pi a\,\Delta\gamma}{E^*}}, \tag{4.19}$$

$$F_N(a) = F_{n.a.}(a) - \sqrt{8\pi E^* a^3 \Delta\gamma}. \tag{4.20}$$

The validity of Eqs. (4.19) and (4.20) is in no way limited to the parabolic contact. They are generally valid for arbitrary axially-symmetric contacts with a simply connected contact area [18].

No additional proof is needed to show that the results of the generalized JKR theory can be mapped to one-dimensional models. This is because if arbitrary axially-symmetric contacts without adhesion (for simply connected contact areas) satisfy the requirements of the reduction method (see Chap. 3), including the flat indenter, then this must also be true for their superposition. The adhesive contact forms a sort of special case of the rule of superposition described in Sect. 3.2, which is valid for the same contact areas. Nevertheless, Sect. 17.3 contains a step-by-step derivation, including information dealing with stability, which is based on the fracture mechanical analogy found by Maugis and Barquins.

The model for the adhesive contact between a parabolic indenter and an elastic half-space is sketched in Fig. 4.1. The loading and unloading process for the one-dimensional model, which exactly describes the equilibrium state of the adhesive contact in three dimensions, is simple. As in the case without adhesion, the equivalent profile g is first calculated and an appropriately formed indenter is subsequently pressed into a one-dimensional linearly elastic foundation with a force $F_{n.a.}$. The springs at the contact boundary $x = \pm a$ exhibit the non-loaded initial length ℓ_o, while the springs within the contact area are under load. Let us now assume that all springs in contact with the indenter adhere to it and for a subsequent decrease in normal force, the contact radius remains unchanged. Going from the contact boundary towards the center, more and more springs are placed under tensile loading. As soon as the change in length of the outer springs reach the maximum allowable value

$$\Delta\ell(\pm a) = \Delta\ell_{\max}(a) := \sqrt{\frac{2\pi a\,\Delta\gamma}{E^*}}, \tag{4.21}$$

there exists an indifference between the states of adhesion and separation. At the points $x = \pm a$, the surface displacement for the one-dimensional model is

$$u_z(\pm a) = -\Delta\ell_{\max}(a). \tag{4.22}$$

This state corresponds exactly to that of the equilibrium state in the three-dimensional case of adhesive contact. The separation condition (4.21) is a type of *local* fracture criterion for the equivalent model, which is also known as the

rule of Heß for the adhesive contact [6, 19]. Alternately, we can define a maximum spring force instead of a maximum change in length. Upon exceeding this force, the springs at the boundary separate. Especially for the numerical application, the dependence of the separation condition on the contact half-width should be taken into account.

Even the stability of the equilibrium state can be investigated very trivially under various boundary conditions within the framework of the reduction method. For this (referring to Sect. 17.3), the following inequality is used:

$$\frac{\Delta\ell_{\max}(a)}{a} \leq k\frac{\partial g(a)}{\partial a} \quad \text{with } k = \begin{cases} 2/3 & \text{for } F_N = const. \\ 2 & \text{for } d = const. \end{cases} . \tag{4.23}$$

The equals sign in (4.23) defines the state of marginal stability, which allows for the critical values to be calculated. According to (4.23), the slope of the equivalent profile at the point $x = a$ determines the stability of the system. Depending on the boundary condition (*fixed-load* or *fixed-grips*), it is to be multiplied with the corresponding factor k and compared with the quotient of the separation length and contact radius.

With the exception of the stability considerations named above, the implementation of adhesion using the reduction method requires no additional effort whatsoever. In contrast to the non-adhesive contact, only the displacement in the one-dimensional model must be extended by the rigid-body portion (see Fig. 4.1)

$$u_z(x) := d(a) - g(x) = g(a) - g(x) - \Delta\ell_{\max}(a) \quad \text{for } 0 \leq |x| \leq a. \tag{4.24}$$

The indentation depth is defined by the displacement at $x = 0$:

$$d(a) := u_z(0) = g(a) - \Delta\ell_{\max}(a). \tag{4.25}$$

By taking (4.24) and (4.25) into account, the normal force is obtained as a function of the contact radius in the same way as before, from the sum of the spring forces:

$$F_N(a) := E^* \int_{-a}^{a} u_z(x)\mathrm{d}x. \tag{4.26}$$

The normal stresses in the contact area are obtained also in the same way as in the contact without adhesion, from the modified Abel integral of the vertical distributed load:

$$\sigma_{zz}(r) = \frac{1}{\pi}\int_r^a \frac{q'(x)}{\sqrt{x^2 - r^2}}\,\mathrm{d}x - \frac{1}{\pi}\frac{q(a)}{\sqrt{a^2 - r^2}} \quad \text{with} \quad q(x) = E^* u_z(x). \tag{4.27}$$

In order to make the simple steps of the reduction method clear to the reader, we will show the complete mapping of the original theory from Johnson, Kendall, and Roberts as an example. In the typical way, the equivalent profile g of the parabolic

indenters with the radius of curvature must first be determined. According to the *rule of Popov*, we must simply divide the radius of curvature by two:

$$f(r) = \frac{r^2}{2R} \Rightarrow g(x) = \frac{x^2}{R} \cdot \tag{4.28}$$

The surface displacement in the equivalent model, according to Eq. (4.24), is

$$u_z(x) = \frac{a^2 - x^2}{R} - \Delta\ell_{\max}(a), \tag{4.29}$$

from which we can determine the indentation depth with respect to contact radius according to (4.25). Taking the separation condition (4.21) into account, we obtain

$$d(a) = \frac{a^2}{R} - \sqrt{\frac{2\pi a\,\Delta\gamma}{E^*}}. \tag{4.30}$$

The normal force is the sum of the spring forces

$$F_N(a) = E^* \int_{-a}^{a} u_z(x)\mathrm{d}x = 2E^* \int_0^a \left(d - \frac{x^2}{R}\right)\mathrm{d}x = \frac{4}{3}E^*\frac{a^3}{R} - \sqrt{8\pi a^3 E^* \Delta\gamma}. \tag{4.31}$$

Equations (4.30) and (4.31) will seem familiar to the reader, for they are exactly those developed by Johnson, Kendall, and Roberts using the minimum in the total energy.

We investigate the stability of the system with the criterion (4.23). For this, let k not be fixed for the time being. The slope of the equivalent profile at the point $x = a$ is

$$g(a) = \frac{a^2}{R} \Rightarrow \frac{\partial g(a)}{\partial a} = \frac{2a}{R}. \tag{4.32}$$

Insertion of (4.32) into (4.23) and taking the separation condition (4.21) into account, results in

$$\sqrt{\frac{2\pi a\,\Delta\gamma}{E^*}}\frac{1}{a} \le k\frac{2a}{R}, \tag{4.33}$$

and after simple rearrangement, the contact radii for which the system is stable are obtained:

$$a \ge \left(\frac{\pi R^2 \Delta\gamma}{2k^2 E^*}\right)^{1/3} \quad \text{marginal stability: } a_c(k) = \left(\frac{\pi R^2 \Delta\gamma}{2k^2 E^*}\right)^{1/3}. \tag{4.34}$$

The marginally stable case characterizes the critical state at which the calculation of the critical values is possible: the minimum normal force and minimum indentation depth. In order to accomplish this, the contact radius in Eq. (4.34) must be take into account in Eqs. (4.30) and (4.31), from which we obtain

$$F_c(k) = \left(\frac{1}{3k} - 1\right)\frac{2\pi R\,\Delta\gamma}{k} \text{ and } d_c(k) = \left(\frac{1}{k} - 2\right)\left(\frac{\pi^2 R\,\Delta\gamma^2}{4k\,E^{*^2}}\right)^{1/3}. \tag{4.35}$$

Until now, we have left the type of boundary condition open. Now, we will assign the variable k a value. Under the *fixed-load* condition, we must set $k = \frac{2}{3}$ and obtain the known results:

$$a_c = \left(\frac{9\pi R^2 \Delta\gamma}{8E^*}\right)^{1/3}, \; F_c = -\tfrac{3}{2}\pi R\,\Delta\gamma\,, \; d_c = -\left(\frac{3\pi^2 R\,\Delta\gamma^2}{64E^{*2}}\right)^{1/3}. \quad (4.36)$$

The critical force in (4.36) is also called the *adhesion force* and corresponds to the minimum in the normal force. Its magnitude, however, is called the *maximum separation force.* Under the *fixed-grips* condition ($k = 2$), the indentation depth is actually able to be *stably* decreased even further, until the following three relationships are reached:

$$a_{c,d} = \left(\frac{\pi R^2 \Delta\gamma}{8E^*}\right)^{1/3}, \; F_{c,d} = -\tfrac{5}{6}\pi R\,\Delta\gamma\,, \; d_{c,d} = -\tfrac{3}{4}\left(\frac{\pi^2 R\,\Delta\gamma^2}{E^{*2}}\right)^{1/3}, \quad (4.37)$$

The additional index "d" denotes the fixed-grips condition.

For the sake of completeness, let the equilibrium curves (4.30) and (4.31) be expanded by a normalized representation. With the respect to the magnitude, the critical values are

$$\tilde{F}_N(\tilde{a}) = \tilde{a}^3 - 2\tilde{a}^{3/2} \text{ and } \tilde{d}(\tilde{a}) = 3\tilde{a}^2 - 4\tilde{a}^{1/2}, \quad (4.38)$$

with $\tilde{F}_N := F_N/|F_c|$, $\tilde{d} := d/|d_c|$, and $\tilde{a} := a/a_c$. Because of their complexity due to the normal force as a function of the indentation depth, they will not be specified explicitly, but their trends will be graphically shown with the help of the parametric form (4.38). Figure 4.6a shows the trend compared to the adhesive contact of a conical profile (shown in Fig. 4.6b). The dashed ends of the functions mark the extended domain of stability under the *fixed-grips* condition.

Comparing the curves reveals that the adhesion forces are negative in both cases, but the critical indentation depths (at a constant force) have different signs. The solution of the adhesive conical contact and the confirmation of the corresponding curves from Fig. 4.6b is one of the problems at the end of this chapter.

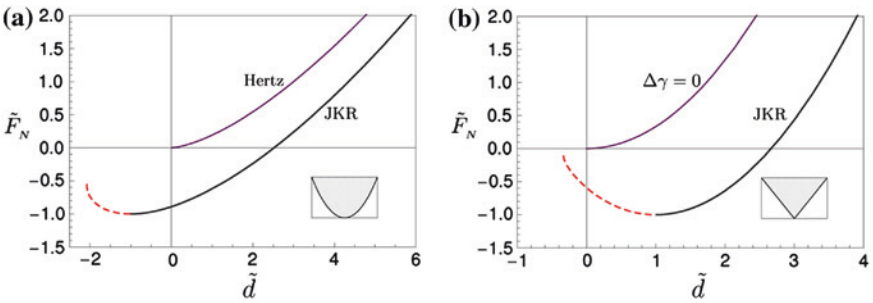

Fig. 4.6 Dependence of the normalized force on the normalized indentation depth for the adhesive contact for a parabolic (**a**) and a conical indenter (**b**); for comparison purposes, the trends of the respective contacts without adhesion are shown

Only the calculation of the stress is now needed to completely solve the adhesive contact problem for parabolic profiles. For this, we need the linear force density in the equivalent model:

$$q(x) = E^* u_z(x) = E^* \left[\frac{a^2 - x^2}{R} - \Delta\ell_{\max}(a) \right]. \tag{4.39}$$

By differentiating this with respect to x and then inserting the value at $x = a$, we obtain

$$q'(x) = -\frac{2E^*}{R} x \text{ and } q(a) = -E^* \Delta\ell_{\max}(a)\,. \tag{4.40}$$

Insertion of (4.40) into (4.27) results initially in

$$\sigma_{zz}(r) = -\frac{2E^*}{\pi R} \int_r^a \frac{x}{\sqrt{x^2 - r^2}}\,\mathrm{d}x + \frac{E^*}{\pi} \frac{\Delta\ell_{\max}(a)}{\sqrt{a^2 - r^2}}, \tag{4.41}$$

which is then integrated and suitably normalized, resulting in

$$\frac{\sigma_{zz}(s)}{\bar{p}_{n.a.}} = -\frac{3}{2}\sqrt{1 - s^2} + \frac{1}{2}\left(1 - \frac{F_N}{F_{n.a.}}\right) \frac{1}{\sqrt{1 - s^2}} \text{ with } s := \frac{r}{a} \text{ and } \bar{p}_{n.a.} := \frac{F_{n.a.}}{A}\,. \tag{4.42}$$

For the critical state of $F_c := F_N(a_c) = -F_{n.a.}$, this stress curve is presented in Fig. 4.5b.

The process for mapping the classical contact problems described by Johnson, Kendall, and Roberts within the reduction method may seem a bit challenging at first. However, the reader will quickly be convinced that, in reality, the opposite is the case. The method is composed primarily of just a few steps, which are formulated in Eqs. (4.21)–(4.27) and cannot be simpler. In the next section, the method will be used on a more complicated contact problem, which occasionally allows for commentary on the influence of roughness on adhesion.

4.5 Example: Adhesion of a Sphere with a Superimposed Radial Waveform

It is generally known that the adhesion between (visco-) elastic bodies is significantly influenced by the roughness of their surfaces. In the most general cases, the adhesion decreases rapidly with an increase in roughness, however, there are well-founded experimental results [20, 21], which show effects to the contrary. According to this, very soft materials having small scales of roughness exhibit a temporary increase in adhesion before a continuous decrease begins. An established theoretical reason for this increase is based on the increase in the real contact area, which occurs due to viscoelastic creep processes. A further cause for the increase in adhesion was brought to attention by Guduru [22] by theoretically

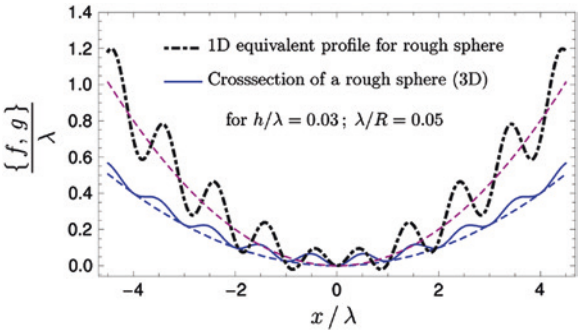

Fig. 4.7 Profile cross-section of a parabolic body superimposed with a radial waveform and its one-dimensional equivalent

investigating the adhesive, elastic contact between a half-space and a parabolic body with superimposed axially-symmetric waveforms. Due to the waveform, defined oscillations occur in the equilibrium curves, bringing about instabilities during the separation process. These instabilities can lead to a significant increase in the separation force. Experimental investigations [23] confirm the validity of the theoretical ansatz from Guduru, which requires a simply connected contact area at the beginning of the separation process. This last condition, along with that of axial-symmetry, allow this example for a rough contact to be *exactly* mapped using the method of dimensionality reduction, which will be the subject of the following considerations.

The axially-symmetric profile is composed of a parabolic base profile with a radius of curvature of R and a radially harmonic profile with the wavelength λ and the (roughness) amplitude h according to the equation[4]

$$f(r) = \frac{r^2}{2R} + h\left[1 - \cos\left(\frac{2\pi}{\lambda}r\right)\right]. \tag{4.43}$$

The cross-section of the profile in the x-z plane for $h/\lambda = 0.03$ and $\lambda/R = 0.05$ is shown in Fig. 4.7. A simply connected contact area at *every* point in time for the indentation and separation process requires a monotonically increasing profile for $r \geq 0$, which with the help of the derivative

$$f'(r) = \frac{r}{R} + h\frac{2\pi}{\lambda}\sin\left(\frac{2\pi}{\lambda}r\right), \tag{4.44}$$

is expressed by the following condition:

$$f'(r) \geq 0 \Rightarrow \alpha := \frac{\lambda^2}{hR} \geq 4\pi^2 \sup\left[\frac{-\sin\left(\frac{2\pi}{\lambda}r\right)}{\frac{2\pi}{\lambda}r}\right] \approx 8.576. \tag{4.45}$$

[4] It is irrelevant if the superimposed profile is pressed into a planar elastic half-space or a parabolic body is pressed into an elastic half-space with the corresponding waveform.

Although the monotonic requirement (4.45) is obviously not met by the profile in Fig. 4.7 ($\alpha \approx 1.667 < 8.576$), a simply connected contact area can nevertheless be realized for a sufficiently large normal force. The reason for this is the decrease in the least upper bound (supremum) in (4.45), if we constrict ourselves to sufficiently large $r > r_{crit}$.

In order to determine the one-dimensional equivalent profile, we must make use of the conversion formula (see Sect. 3.3).

$$g(x) := |x| \int_0^{|x|} \frac{f'(r)}{\sqrt{x^2 - r^2}} \mathrm{d}r = \frac{x^2}{R} + s(x)h \int_0^{s(x)} \frac{\sin(u)}{\sqrt{s(x)^2 - u^2}} \mathrm{d}u \quad \text{with} \quad s(x) = \frac{2\pi}{\lambda}|x|. \tag{4.46}$$

The integral on the right side leads to the Struve function, so that we obtain

$$g(x) = \frac{x^2}{R} + \frac{\pi^2}{\lambda}|x|h \cdot H_0\left(\frac{2\pi}{\lambda}|x|\right) \tag{4.47}$$

for the equivalent profile. Let us here mention that the series representation of the Struve function is

$$H_n(x) = \sum_{k=0}^{\infty} \frac{(-1)^k}{\Gamma\left(k + \frac{3}{2}\right)\Gamma\left(k + n + \frac{3}{2}\right)} \left(\frac{x}{2}\right)^{2k+n+1}. \tag{4.48}$$

The one-dimensional equivalent profile according to Eq. (4.47) is likewise presented in Fig. 4.7. Moreover, the original and equivalent profiles are shown for a roughness of zero (dashed lines) and present, of course, a constant vertical scaling relationship based on the rule of Popov.

Upon obtaining the one-dimensional profile, the three-dimensional problem is as good as solved, because now the modified profile must simply be pressed with sufficient force into the one-dimensional layer of springs and then the force reduced while taking the equilibrium condition (4.22) and the accompanying stability test (4.23) into account. The numerical implementation is trivial due to the independence of the spring displacement, but nevertheless, agrees exactly with the three-dimensional theory! In the following, we conduct an analytical approach, which leads to the indentation depth when Eq. (4.47) is taken into account:

$$d(a) := g(a) - \Delta\ell_{\max}(a) = \frac{a^2}{R} + \frac{\pi^2 ah}{\lambda} H_0\left(\frac{2\pi}{\lambda}a\right) - \sqrt{\frac{2\pi a\,\Delta\gamma}{E^*}}. \tag{4.49}$$

The surface displacement of the linearly elastic foundation is defined by the difference between the indentation depth d and the equivalent profile g. Except for

the sign, this displacement corresponds to the change in length of the springs. The resulting spring forces must maintain equilibrium by summation with the normal force:

$$F_N(a) = E^* \int_{-a}^{a} \big[d - g(x)\big]\,\mathrm{d}x. \tag{4.50}$$

Insertion of (4.47) and (4.49) into (4.50) results in

$$F_N(a) = \frac{4}{3}E^*\frac{a^3}{R} + E^*\pi a h\left[\frac{2\pi a}{\lambda}H_0\left(\frac{2\pi a}{\lambda}\right) - H_1\left(\frac{2\pi a}{\lambda}\right)\right] - \sqrt{8\pi a^3 E^* \Delta\gamma} \tag{4.51}$$

after integration and simple rearrangement. By taking the normalized values suggested by Guduru [22] into account:

$$\bar{F}_N := \frac{2F_N}{3\pi R\Delta\gamma}\,,\ \bar{d} := \frac{d}{\lambda}\,,\ \bar{a} := \frac{a}{\lambda}\,,\ \bar{\lambda} := \frac{\lambda}{R}\,,\ \bar{h} := \frac{h}{\lambda}\,,\ \overline{\Delta\gamma} := \frac{2\pi\Delta\gamma}{E^*R}$$

the equilibrium relations (4.49) and (4.51) can be expressed in dimensionless form:

$$\bar{d}\left(\bar{a};\bar{\lambda};\bar{h};\overline{\Delta\gamma}\right) = \bar{a}^2\bar{\lambda} + \pi^2\bar{a}\,\bar{h}\cdot H_0(2\pi\bar{a}) - \sqrt{\frac{\bar{a}\,\overline{\Delta\gamma}}{\bar{\lambda}}}, \tag{4.52}$$

$$\bar{F}_N\left(\bar{a};\bar{\lambda};\bar{h};\overline{\Delta\gamma}\right) = \frac{16}{9}\frac{\bar{a}^3\bar{\lambda}^3}{\overline{\Delta\gamma}} + \frac{4\pi}{3}\frac{\bar{a}\,\bar{h}\bar{\lambda}^2}{\overline{\Delta\gamma}}[2\pi\bar{a}\cdot H_0(2\pi\bar{a}) - H_1(2\pi\bar{a})] - \frac{8}{3}\sqrt{\frac{\bar{a}^3\bar{\lambda}^3}{\overline{\Delta\gamma}}}. \tag{4.53}$$

With the normalized contact radius $\bar{a}$ as a parameter, the (normalized) normal force can be plotted as a function of the (normalized) indentation depth. Figure 4.8 shows this plot for the parameters

$$\bar{h} = 0.005\,,\ \bar{\lambda} = 0.05\,,\ \overline{\Delta\gamma} = 0.05, \tag{4.54}$$

which only exhibits slight oscillating deviations in the equilibrium curve compared to the parabolic contact without roughness. The monotonic condition (4.45) is satisfied regardless of the load at any point in time.

If we now increase the size of the roughness and keep all other values the same, then a significant change occurs in the equilibrium curve. Oscillations of strong amplitude occur and can lead to an increase in the maximum separation force. Figure 4.9 presents this curve for the profile discussed at the beginning of this section (see Fig. 4.7), which is characterized by a roughness six times larger. The maximum separation force is increased by about 19 % with respect to the parabolic base profile. The critical indentation depth can be decreased by a further 10 % by using the fixed grips condition. Furthermore, the equilibrium curves are

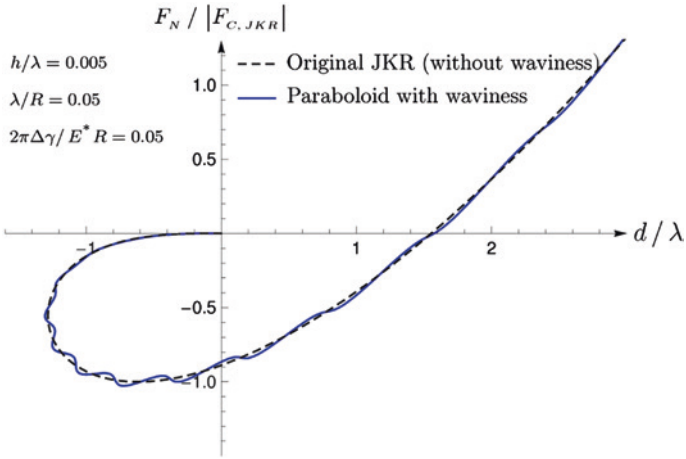

Fig. 4.8 Normal force with respect to the indentation depth for the adhesive contact of a parabolic profile with a superimposed radial waveform. The (small) roughness $h = 0.005\,\lambda$ causes only a minor difference from the original trend of the JKR theory

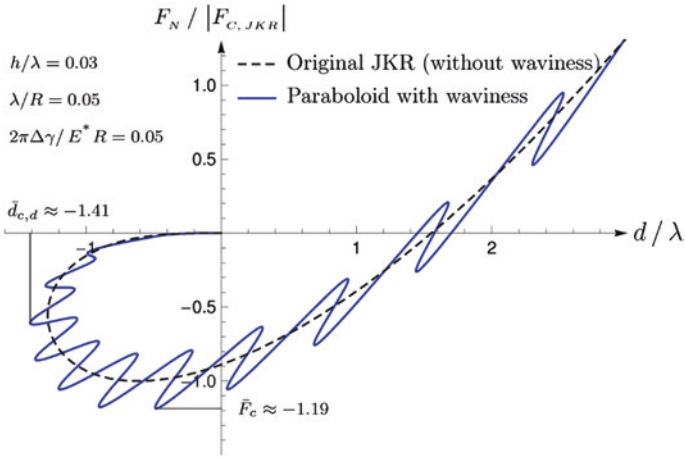

Fig. 4.9 Normal force with respect to the indentation depth for the adhesive contact with a superimposed radial waveform. The assumed roughness of $h = 0.03\,\lambda$ causes strong oscillations, resulting in an additional increase in the adhesion force of about 19 % compared to the original JKR theory

not continuous throughout the separation process. Due to the constant switching from stable to unstable domains, finite jumps occur, which result in energy loss.

As mentioned earlier, the exact solution of contact problems using the method of dimensionality reduction requires a simply-connected contact area and cannot be immediately transferred to partial contacts. Furthermore, the superimposed

waveforms must be axially-symmetric. If one of these requirements is not met, significantly divergent results can result. For example, if a planar waveform instead of a radial waveform is present, then there will be no jumps in the equilibrium curve [24].

4.6 Problems

Problem 1 Investigate the contact between an elastic half-space and a conical body defined by $f(r) = \tan\theta \cdot r$. Adhesion forces should be taken into account. Determine the indentation depth and the normal force with respect to the contact radius. Furthermore, determine the critical values under the *fixed-load* conditions and the equilibrium relations in dimensionless parameters.

Solution The equivalent one-dimensional profile is obtained by vertically scaling the original profile by a factor of $\kappa_1 = \pi/2$ and is equal to $g(x) = (\pi/2)\tan\theta \cdot |x|$. From (4.24), the surface displacement can be obtained for the equivalent profile:

$$u_z(x) = g(a) - g(x) - \Delta\ell_{\max}(a) = \frac{\pi}{2}\tan\theta \cdot (a - |x|) - \Delta\ell_{\max}(a). \tag{4.55}$$

The indentation depth is the displacement at the point $x = 0$:

$$d(a) := u_z(0) = \frac{\pi}{2}\tan\theta \cdot a - \Delta\ell_{\max}(a) = \frac{\pi}{2}\tan\theta \cdot a - \sqrt{\frac{2\pi a\,\Delta\gamma}{E^*}}. \tag{4.56}$$

The sum of the spring forces must counteract the normal force:

$$F_N(a) = E^* \int_{-a}^{a} u_z(x)\mathrm{d}x = 2E^* \int_{0}^{a} \big[d - g(x)\big]\mathrm{d}x = \frac{1}{2}\pi E^* \tan\theta \cdot a^2 - \sqrt{8\pi a^3 E^* \Delta\gamma}. \tag{4.57}$$

We take the condition for calculating the critical contact radius a_c at a constant contact radius from Eq. (4.23):

$$\frac{\Delta\ell_{\max}(a_c)}{a_c} = \frac{2}{3}\frac{\partial g(a)}{\partial a}\bigg|_{a=a_c} \quad \text{with} \quad \frac{\partial g(a)}{\partial a} = \frac{\pi}{2}\tan\theta\,, \tag{4.58}$$

for which the right hand side is already extended by the slope of the profile at hand. By using the rule of Heß, the critical contact radius is obtained. Insertion of this value into the equilibrium relationships (4.56) and (4.57) and then rearranging the equations results in the adhesion force and the critical indentation depth:

$$a_c = \frac{18\,\Delta\gamma}{\pi\tan^2\theta \cdot E^*},\; F_c = -\frac{54\,\Delta\gamma^2}{\pi\tan^3\theta \cdot E^*},\; d_c = \frac{3\,\Delta\gamma}{\tan\theta \cdot E^*}\cdot \tag{4.59}$$

By introducing the normalized values $\tilde{F}_N := F_N/|F_c|$, $\tilde{d} := d/|d_c|$, and $\tilde{a} := a/a_c$, we obtain the equilibrium relationships (4.56) and (4.57) in dimensionless form:

$$\tilde{F}_N(\tilde{a}) = 3\tilde{a}^2 - 4\tilde{a}^{3/2} \text{ and } \tilde{d}(\tilde{a}) = 3\tilde{a} - 2\tilde{a}^{1/2}. \tag{4.60}$$

With the help of the parametric equations in (4.60), the normalized force can be easily plotted as a function of normalized indentation depth, which is shown in Fig. 4.6b. The comparison with the parabolic contact shows, above all, a striking difference in the critical indentation depth (under *fixed-load* conditions), which have opposing signs. All of the results for this exercise mirror the three-dimensional theory exactly (see [14]).

Problem 2 Determine the maximum separation force for the elastic contact between a flat, cylindrical indenter with the radius a and a half-space.

Solution From the original profile $\mathrm{f}(r) = 0$, the equivalent profile $g(x) = 0$ is directly obtained, so that the surface displacement within the contact area corresponds everywhere to the indentation depth according to (4.24). This means that

$$u_z(x) = d(a) = -\Delta\ell_{\max}(a) = -\sqrt{\frac{2\pi a\,\Delta\gamma}{E^*}}\,. \tag{4.61}$$

Because all of the springs exhibit the same change in length based on (4.61), the calculation of the normal force is trivial:

$$F_N(a) = -2E^* a\,\Delta\ell_{\max}(a) = -\sqrt{8\pi a^3 E^* \Delta\gamma}. \tag{4.62}$$

The verification of the condition (4.23), however, uncovers the fact that a stable, quasi-static equilibrium in the form of a controlled fracture is not possible. Therefore, all of the springs will adhere to the indenter until they reach the change in length of (4.61) and then simultaneously separate (*complete rupture)*. The normal force according to (4.62) presents simultaneously the adhesion force and the magnitude of the maximum separation force

$$F_A := |F_N(a_c)| = \sqrt{8\pi a^3 E^* \Delta\gamma}, \tag{4.63}$$

which corresponds with the known result of Kendall [7].

Problem 3 Analyze the influence of the profile form on the adhesion force for a single contact within a biological system. For this, assume an axially-symmetric profile in the form of a power function with a positive real exponent according to

$$f(r) = C \cdot r^n \text{ with } n \in \mathbb{R}^+\,. \tag{4.64}$$

In the first step, identify the equilibrium relationships $F_N(a)$ and $d(a)$. Then, calculate the critical values for marginal stability from (4.23) for a *constant normal force* and non-dimensionalize the equilibrium relationships.

Solution We obtain the one-dimensional equivalent profile by using the generalized rule of Heß (see Sect. 3.2):

$$g(x) = \kappa_n f(|x|) = \kappa_n C|x|^n \text{ with } \kappa_n = \frac{\sqrt{\pi}}{2}\frac{n\Gamma(\frac{n}{2})}{\Gamma(\frac{n+1}{2})}. \tag{4.65}$$

The difference between the value of the function for the equivalent profile at the contact boundary and the separation length provides the indentation depth

$$d(a) = g(a) - \Delta\ell_{\max}(a) = \kappa_n C a^n - \sqrt{\frac{2\pi a\,\Delta\gamma}{E^*}}. \tag{4.66}$$

The surface displacement in the one-dimensional model is then

$$u_z(x) := d - g(x) = \kappa_n C\left(a^n - |x|^n\right) - \sqrt{\frac{2\pi a\,\Delta\gamma}{E^*}}, \tag{4.67}$$

which expresses, except for the sign, the change in length of the individual springs. After multiplication with the stiffness and summation over the contact length, the normal force is found:

$$F_N(a) = 2E^* \int_0^a \left[d - g(x)\right] dx = 2E^* \frac{n}{n+1}\kappa_n C a^{n+1} - \sqrt{8\pi a^3 E^* \Delta\gamma}. \tag{4.68}$$

The critical contact radius is obtained from the (transformed) stability equation for the one-dimensional model. It requires only (!) that the profile slope at the contact boundary be known, which is given here by

$$\frac{\partial g(a)}{\partial a} = n\,\kappa_n C a^{n-1}. \tag{4.69}$$

Insertion into (4.23) leads to the critical contact radius

$$\frac{\Delta\ell_{\max}(a_c)}{a_c} = \frac{2}{3} n\,\kappa_n C a_c^{n-1} \;\Rightarrow\; a_c = \left(\frac{9\pi\,\Delta\gamma}{2n^2\kappa_n^2 C^2 E^*}\right)^{\frac{1}{2n-1}}, \tag{4.70}$$

which provides the adhesion force and the critical indentation depth when inserted into the equilibrium relationships:

$$F_c = \frac{1-2n}{n+1}\left[\left(\frac{3}{2n\kappa_n C}\right)^3 (2\pi\,\Delta\gamma)^{n+1} E^{*\,n-2}\right]^{\frac{1}{2n-1}}, \tag{4.71}$$

$$d_c = \left(1 - \frac{2}{3}n\right)\left[\frac{9\pi\,\Delta\gamma}{2n^2 E^*}\left(\frac{1}{\kappa_n C}\right)^{1/n}\right]^{\frac{n}{2n-1}}. \tag{4.72}$$

If normalized by the magnitudes of the critical values $\tilde{F}_N := F_N/|F_c|$, $\tilde{d} := d/|d_c|$, and $\tilde{a} := a/a_c$, the equilibrium relationship exhibit an especially simple structure

$$\tilde{F}_N(\tilde{a}) = \frac{1}{|1-2n|}\left[3\tilde{a}^{n+1} - 2(n+1)\tilde{a}^{3/2}\right] \text{ and } \tilde{d}(\tilde{a}) = \frac{1}{|3-2n|}\left(3\tilde{a}^{n} - 2n\tilde{a}^{1/2}\right). \tag{4.73}$$

For $n = 1$, the results correspond to those from Problem 1, while for $n = 2$, the classical results from JKR theory are obtained. The calculation of the critical contact radius as well as the adhesion force go back to Yao and Gao [25] and were actually employed to investigate adhesion in biological structures [26]. Extended stability considerations can be found in the work by Heß [6].

Problem 4 Determine the normal force and indentation depth with respect to the contact radius for the adhesive normal contact between a sphere with the radius R and an elastic half-space. In contrast to the parabolic profile approximation in JKR theory, the exact spherical form should be considered. Simultaneously, it is assumed that only small deformations take place and the material is linearly elastic.

Solution This contact problem was already solved in Problem 8 in Chap. 3 for the case without adhesion. Referring to this exercise, we can simply take the explicitly calculated equivalent profile:

$$f(r) = R - \sqrt{R^2 - r^2} \Rightarrow g(x) = \frac{1}{2}x\ln\left(\frac{R+x}{R-x}\right). \tag{4.74}$$

By subtracting the separation length from the value of the function of the equivalent profile at the contact boundary, we obtain the indentation depth

$$d(a) = g(a) - \Delta 1_{\max}(a) = \frac{1}{2}a\ln\left(\frac{R+a}{R-a}\right) - \sqrt{\frac{2\pi a\,\Delta\gamma}{E^*}}. \tag{4.75}$$

The displacement in the one-dimensional model is then

$$u_z(x) := d - g(x) = \frac{1}{2}a\ln\left(\frac{R+a}{R-a}\right) - \sqrt{\frac{2\pi a\,\Delta\gamma}{E^*}} - \frac{1}{2}x\ln\left(\frac{R+x}{R-x}\right). \tag{4.76}$$

The calculation of the normal force requires the summation of the contributions from the individual springs and can be immediately given with the help of the solution of the contact without adhesion as

$$F_N(a) = E^*\int_{-a}^{a} u_z(x)\mathrm{d}x = E^*\frac{R^2+a^2}{2}\ln\left(\frac{R+a}{R-a}\right) - E^*Ra - \sqrt{8\pi a^3 E^*\Delta\gamma}. \tag{4.77}$$

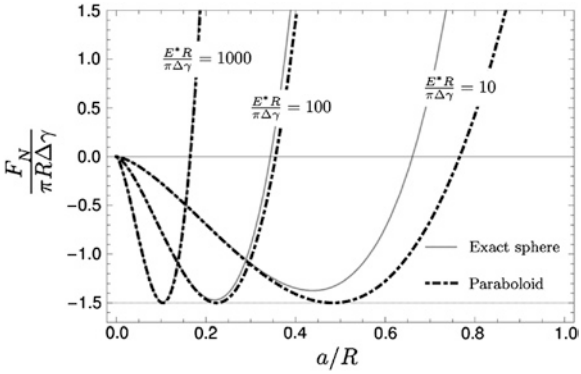

Fig. 4.10 Normal force as a function of contact radius in the normalized presentation for the adhesive contact: Comparison between the parabolic approximation and the exact spherical profile for various values of $m = E^* R/(\pi \Delta\gamma)$

By introducing the normalized values $\tilde{F}_N := \frac{F_N}{\pi R \Delta\gamma}$ and $\tilde{a} = \frac{a}{R}$ as well as the parameter $m := \frac{E^* R}{\pi \Delta\gamma}$, we can convert Eq. (4.77) into the dimensionless form

$$\tilde{F}_N(\tilde{a}) = \frac{1}{2} m \left(1 + \tilde{a}^2\right) \ln\left(\frac{1+\tilde{a}}{1-\tilde{a}}\right) - m\tilde{a} - \sqrt{m}(2\tilde{a})^{3/2}. \tag{4.78}$$

The derived relationships agree exactly to those of the three-dimensional theory developed by Maugis [27]. For comparative purposes, let the respective normalized form of the JKR equation for a parabolic profile be noted:

$$\tilde{F}_N(\tilde{a}) = \frac{4}{3} m\tilde{a}^3 - \sqrt{m}(2\tilde{a})^{3/2}. \tag{4.79}$$

Figure 4.10 emphasizes the difference between the spherical contact and the corresponding parabolic approximation. For large values of the parameter m ($m > 1,000$), they agree well with one another, while for smaller values of m, significant deviations are apparent. The maximum separation force is then especially dependent on the elastic properties. The parabolic approximation appears to give acceptable results over several orders of magnitude of the parameter m up to a contact radius of $a \approx 0.2R$.

With these results, Maugis attempted to describe the contact for small spheres with that of a very soft elastic solid and in this way, proved the invalidity of the parabolic approximation if the contact radius is on the same order of magnitude as the radius of curvature. In this regime, however, the application of the theory of linear elasticity is highly questionable, which Lin and Chen [28] discovered on the basis of geometric and physical *non-linear* theory and for which Greenwood [29] suggested critical additions.

Problem 5 Determine the indentation depth and the normal force as a function of contact radius for the adhesive contact of the axially-symmetric body shown in Fig. 4.11 with an elastic half-space. The form of the body is described by a parabolic profile with a flattened tip:

$$f(r) = \begin{cases} 0 & \text{for } 0 \le r < b \\ \frac{r^2 - b^2}{2R} & \text{for } b \le r \le a \end{cases}. \tag{4.80}$$

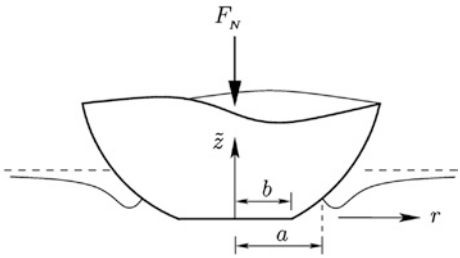

Fig. 4.11 Qualitative presentation of the adhesive contact of a parabolic profile with a flattened tip and an elastic half-space

Solution The corresponding non-adhesive contact problem was solved in Sect. 3.3. It served as an introductory example for the explicit application of the generalized formula (3.27) to determine the equivalent profile, which also composes the first step in the mapping of the contact with adhesion. By taking the derivative of the original profile into account, we obtained

$$g(x) := |x| \int_0^{|x|} \frac{f'(r)}{\sqrt{x^2 - r^2}} \mathrm{d}r = \begin{cases} 0 & \text{for } 0 \le |x| < b \\ \frac{|x|}{R}\sqrt{x^2 - b^2} & \text{for } b \le |x| \le a \end{cases}. \tag{4.81}$$

With the help of (4.81), the indentation depth can be directly given as

$$d(a) := g(a) - \Delta\ell_{\max}(a) = \frac{a}{R}\sqrt{a^2 - b^2} - \sqrt{\frac{2\pi a\,\Delta\gamma}{E^*}}. \tag{4.82}$$

The displacements of the contact points in the linearly elastic foundation are still obtained by the difference between the indentation depth and the value of the equivalent profile and provides the change in length of the spring (with the exception of the sign). Summing the individual spring contributions, leads to the normal force

$$F_N(a) = E^* \int_{-a}^{a} u_z(x)\mathrm{d}x = \frac{2E^*}{3R}\left(2a^2 + b^2\right)\sqrt{a^2 - b^2} - \sqrt{8\pi a^3 E^* \Delta\gamma}. \tag{4.83}$$

The critical values (*fixed load*) in the case of $b = 0$ are those from the original theory for a parabolic body

$$a^* = \left(\frac{9\pi R^2 \Delta\gamma}{8E^*}\right)^{1/3},\ F^* = -\frac{3}{2}\pi R\,\Delta\gamma\,,\ d^* = -\left(\frac{3\pi^2 R\,\Delta\gamma^2}{64E^{*2}}\right)^{1/3}, \tag{4.84}$$

which we took from (4.36) and renamed. By normalizing by their magnitudes, we can convert Eqs. (4.82) and (4.83) into the dimensionless forms

$$\hat{d}(\hat{a}) = 3\hat{a}^2\sqrt{1 - \left(\frac{\hat{b}}{\hat{a}}\right)^2} - 4\hat{a}^{1/2}, \tag{4.85}$$

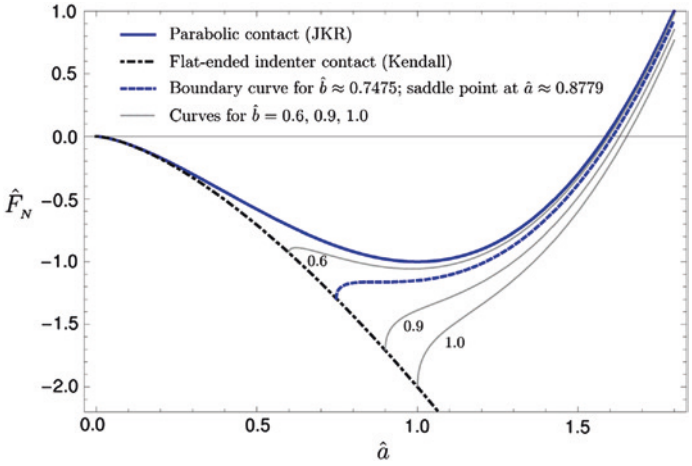

Fig. 4.12 Graphical trends of the normalized normal force as a function of the normalized contact radius for the adhesive contact between a parabolic indenter with a "worn" tip; the parameter b corresponds to the size of the flattened area of the indenter

$$\hat{F}_N(\hat{a}) = \frac{1}{2}\hat{a}^3\left[2 + \left(\frac{\hat{b}}{\hat{a}}\right)^2\right]\sqrt{1 - \left(\frac{\hat{b}}{\hat{a}}\right)^2} - 2\hat{a}^{3/2}, \tag{4.86}$$

where $\hat{F}_N := F_N/|F^*|$, $\hat{d} := d/|d^*|$, $\hat{a} := a/a^*$, and $\hat{b} := b/a^*$ were used for the normalization. In the special case of $\hat{b} = 0$, the resulting equation is (4.38) and for the case of $\hat{b} = \hat{a}$, the resulting equations are (4.61) and (4.62). These cases describe the parabolic contact and the flat indenter contact, respectively. Their graphical trends can be interpreted as extreme values for the general case, which is expressed in Fig. 4.12. Here, unstable domains are not visible. The fact that the horizontal tangents of the minimums of these curves separate the stability domains is clear. It is interesting that for $b > 0.7475\,a^*$, complete separation occurs only after $a = b$, meaning the contact radius corresponds to that of the flattened area of the indenter.

For $b < 0.7475\,a^*$, however, there exists a minimum that marks the adhesion force in a way similar to the parabolic contact. Further considerations, especially those near the boundary curves shown in Fig. 4.12, are contained in [30].

References

1. K.L. Johnson, K. Kendall, A.D. Roberts, Surface energy and the contact of elastic solids. in *Proceedings of the Royal Society of London. Series A, Mathematical and Physical Sciences,* vol. 324, no. 1558 (1971), pp. 301–313
2. B.V. Derjaguin, V.M. Muller, YuP Toporov, Effect of contact deformation on the adhesion of particles. J. Colloid Interface Sci. **55**, 314–326 (1975)
3. R.S. Bradley, The cohesive force between solid surfaces and the surface energy of solids. Philos. Mag. **13**, 853–862 (1932)

4. D. Tabor, Surface forces and surface interactions. J. Colloid Interface Sci. **58**, 2–13 (1977)
5. K.L. Johnson, J.A. Greenwood, An Adhesion Map for the Contact of Elastic Spheres. J. Colloid Interface Sci. **192**, 326–333 (1997)
6. M. Heß, *Über die exakte Abbildung ausgewählter dreidimensionaler Kontakte auf Systeme mit niedrigerer räumlicher Dimension* (Cuvillier, Berlin, 2011)
7. K. Kendall, The adhesion and surface energy of elastic solids. J. Phys. D Appl. Phys. **4**, 1186–1195 (1971)
8. A.A. Griffith, The phenomena of rupture and flow in solids. Philos. Trans. R. Soc. Lond. Ser. A **221**, 163–198 (1921)
9. A.A., Griffith, Theory of rupture. [ed.] Biezeno and Burgers. in *Proceedings of the First International Congress for Applied Mechanics,* 1925, pp. 53–64
10. D. Maugis, M. Barquins, R. Courtel, Griffith Cracks and Adhesion of Elastic Solids. Métaux, Corrosion, Industrie **605**, 1–10 (1976)
11. D. Maugis, M. Barquins, Fracture mechanics and the adherence of viscoelastic bodies. J. Phys. D Appl. Phys. **11**(14), 1989–2023 (1978)
12. G.R. Irwin, Analysis of stresses and strains near the end of a crack traversing a plate. J. Appl. Mech. **24**, 361–364 (1957)
13. Johnson, K.L. Adhesion and friction between a smooth elastic spherical asperity and a plane surface. in *Proceedings of the Royal Society of London. Series A: Mathematical, Physical and Engineering Sciences*, vol. 453, no. 1956. 1997, pp. 163–179
14. D. Maugis, M. Barquins, Adhesive contact of a conical punch on an elastic half-space. Le Journal de Physique Lettres **42**(5), 95–97 (1981)
15. M. Barquins, D. Maugis, Adhesive contact of axisymmetric punches on an elastic half-space: the modified Hertz-Huber's stress tensor for contacting spheres. J. Theor. Appl. Mech. **1**(2), 331–357 (1982)
16. I.N. Sneddon, The relation between load and penetration in the axisymmetric Boussinesq problem for a punch of arbitrary profile. Int. J. Eng. Sci. **3**, 47–57 (1965)
17. K.L. Johnson, A note on the adhesion of elastic solids. British J. Appl. Phys. **9**, 199–200 (1958)
18. D. Maugis, *Contact, adhesion and rupture of elastic solids* (Springer, Berlin, 2000), pp. 213–216
19. M. Heß, On the reduction method of dimensionality: the exact mapping of axisymmetric contact problems with and without adhesion. Phys. Mesomech. **15**(5–6), 264–269 (2012)
20. G.A.D. Briggs, B.J. Briscoe, The effect of surface topography on the adhesion of elastic solids. J. Phys. D Appl. Phys. **10**, 2453–2466 (1977)
21. K.N.G. Fuller, A.D. Roberts, Rubber rolling on rough surfaces. J. Phys. D Appl. Phys. **14**, 221–239 (1981)
22. P.R. Guduru, Detachment of a rigid solid from an elastic wavy surface: Theory. J. Mech. Phys. Solids **55**, 445–472 (2007)
23. P.R. Guduru, C. Bull, Detachment of a rigid solid from an elastic wavy surface: Experiments. J. Mech. Phys. Solids **55**, 473–488 (2007)
24. C. Jin, K. Khare, S. Vajpayee, S. Yang, A. Jagota, C.-Y. Hui, Adhesive contact between a rippled elastic surface and a rigid spherical indenter: from partial to full contact. Soft Matter **7**, 10728–10736 (2011)
25. H. Yao, H. Gao, Optimal shapes for adhesive binding between two elastic bodies. J. Colloid Interface Sci. **298**(2), 564–572 (2006)
26. H. Yao, H. Gao, Mechanical principles of robust and releasable adhesion of gecko. J. Adhes. Sci. Technol. **21**(12–13), 1185–1212 (2007)
27. D. Maugis, Extension of the Johnson-Kendall-Roberts theory of elastic contact of spheres to large contact radii. Langmuir **11**(2), 679–682 (1995)
28. Y.-Y. Lin, H.-Y. Chen, Effect of large deformation and material nonlinearity on the JKR (Johnson-Kendall-Roberts) test of soft elastic materials. J. Polym. Sci. Part B: Polym. Phys. **44**(19), 2912–2922 (2006)
29. J.A. Greenwood, Adhesion of small spheres. Philos. Mag. **89**(11), 945–965 (2009)
30. D. Maugis, M. Barquins, Adhesive contact of sectionally smooth-ended punches on elastic half-spaces: theory and experiment. J. Phys. D Appl. Phys. **16**(10), 1843–1874 (1983)

Chapter 5
Tangential Contact

Markus Heß and Valentin L. Popov

5.1 Introduction

The fundamental property that allows the reduction of three-dimensional contacts to one-dimensional ones is the proportionality of the incremental stiffness to the diameter of the contact area. This property is exhibited by both normal and tangential contacts. The idea behind dimensionality reduction can, therefore, be directly transferred to tangential contacts.

The tangential stiffness of a round contact with the diameter D between two elastic half-spaces is given by the equation [1]

$$k_x = DG^*, \tag{5.1}$$

where G^* is defined as

$$\frac{1}{G^*} = \frac{(2-\nu_1)}{4G_1} + \frac{(2-\nu_2)}{4G_2}. \tag{5.2}$$

G_1 and G_2 denote the shear moduli of the contacting bodies. Thereby, it should be noted that it is assumed that materials are "elastically similar":

$$\frac{1-2\nu_1}{G_1} = \frac{1-2\nu_2}{G_2}, \tag{5.3}$$

which allows the tangential contact problem to be decoupled from the normal contact problem [2]. This condition is identically met for the important case of a contact between a rigid body and an incompressible elastomer (both sides of Eq. (5.3) are zero in this case).

Now, we consider a linearly elastic foundation consisting of springs with the stiffness

$$\Delta k_x = G^* \Delta x, \tag{5.4}$$

V.L. Popov and M. Heß, *Method of Dimensionality Reduction in Contact Mechanics and Friction*, DOI 10.1007/978-3-642-53876-6_5

where Δx is the distance between the springs. The stiffness (5.1) is trivially reproduced with this foundation. In this chapter, we will show that the one-dimensional elastic foundation with the normal stiffness defined in Chap. 3 and the tangential stiffness (5.4) can also be used to *exactly* map tangential contacts with Coulomb friction for *arbitrarily axially-symmetric* profiles. We begin our considerations with the contact between parabolic bodies.

5.2 Tangential Contact with Friction for Parabolic Bodies

We consider a rigid three-dimensional parabolic body with the radius of curvature R that is pressed into an elastic half-space with the normal force F_N and subsequently loaded in the horizontal direction with the force F_x. We assume that the frictional forces acting in the contact can be simply described using Coulomb's law of friction with a constant coefficient of friction μ. From the theory of three-dimensional contact problems, it is known that even the application of an arbitrarily small force results in the formation of a slip domain at the boundary of the contact area, while the inner domain initially sticks [1]. With increasing tangential force, the stick domain shrinks until slip is initiated in the entire contact area. In this section, we investigate the one-dimensional mapping of the aforementioned three-dimensional contact problem (Fig. 5.1).

As before, let the indentation depth of the rigid body into the linearly elastic foundation be denoted by d. The vertical displacement of a spring at a distance x from the middle point of the contact is

$$u_z(x) = d - \frac{x^2}{2R_1}. \tag{5.5}$$

The radius R_1 must be set to $R_1 = R/2$ according to the rules of the reduction method. The elastic force of a single spring at the point x is

$$f_N(x) = E^* u_z(x) \Delta x = \left(d - \frac{x^2}{2R_1} \right) E^* \Delta x. \tag{5.6}$$

The contact radius is obtained from the condition $u_z(a) = 0$:

$$a = \sqrt{2R_1 d} = \sqrt{Rd}. \tag{5.7}$$

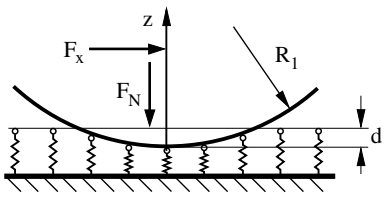

Fig. 5.1 One-dimensional mapping of contact loaded both normally and tangentially

Until now, we have only used the results known from Chap. 3. Now, we denote the horizontal displacement of the parabolic indenter with respect to the foundation with u_x. Then, the horizontal component of the force acting on a sticking spring is

$$f_x(x) = \Delta k_x u_x = G^* \Delta x \cdot u_x. \tag{5.8}$$

We determine the boundary of the sticking domain $x = \pm c$ from the condition that the tangential force achieves its maximum value:

$$f_x(c) = \mu f_N(c) \tag{5.9}$$

or

$$G^* \Delta x \cdot u_x = \mu \left(d - \frac{c^2}{2R_1} \right) E^* \Delta x. \tag{5.10}$$

From this, it follows that

$$c^2 = 2R_1 \left(d - \frac{G^*}{E^*} \frac{u_x}{\mu} \right). \tag{5.11}$$

Solving with respect to u_x results in

$$u_x = \mu \frac{E^*}{G^*} \left(d - \frac{c^2}{2R_1} \right) = \mu \frac{E^*}{G^*} \left(d - \frac{c^2}{R} \right). \tag{5.12}$$

This result agrees with the result for the three-dimensional contact problem [1].

The slip condition outside of the sticking domain means that every point here fulfills Coulomb's law of friction:

$$f_x(x) = \mu f_N(x) \quad \text{for} \quad c < |x| < a. \tag{5.13}$$

Now, we calculate the normal and tangential forces acting in the entire contact area. For the normal force, we once again obtain the Hertzian result:

$$F_N = \int_{-a}^{a} \left(d - \frac{x^2}{2R_1} \right) E^* \mathrm{d}x = \frac{4}{3} E^* (2R_1)^{1/2} d^{3/2} = \frac{2E^* a^3}{3R_1}. \tag{5.14}$$

The tangential force is calculated as

$$F_x = 2 \int_0^c G^* u_x \mathrm{d}x + 2 \int_c^a \mu \left(d - \frac{x^2}{2R_1} \right) E^* \mathrm{d}x = \frac{2E^* a^3 \mu}{3R_1} \left(1 - \left(\frac{c}{a} \right)^3 \right) = \mu F_N \left(1 - \left(\frac{c}{a} \right)^3 \right). \tag{5.15}$$

From this, the relationship between the loading and the radius of the contact area can be determined:

$$\frac{c}{a} = \left(1 - \frac{F_x}{\mu F_N} \right)^{1/3}. \tag{5.16}$$

This result also agrees exactly with that of the three-dimensional problem [1].

We obtain the displacement above which the entire contact area exhibits slip by inserting $c = 0$ into Eq. (5.12):

$$u_{x,\max} = u_x = \mu \frac{E^*}{G^*} d, \tag{5.17}$$

which, of course, also agrees exactly with that of the three-dimensional case.

5.3 Tangential Contact with Friction for Arbitrary Axially-Symmetric Bodies

In the last section, it was proven that the tangential contact with partial slip for two parabolic bodies can be exactly mapped using the method of dimensionality reduction. The generalization to tangential contacts of arbitrarily formed, axially-symmetric bodies is the topic of this chapter; the complete proofs including all assumptions can be found in Chap. 18.

In order to solve the classical three-dimensional contact problem, Cattaneo [3] and Mindlin [4] initially calculated the tangential displacement in the direction of the applied tangential force, which results from the state of full slip. Subsequently, they superimposed the corresponding tangential stress distribution with a second one of the same form, but with the opposite direction. In this way, constant tangential displacements were obtained for an inner circular area and the tangential stresses in the outer domain that are proportional to the normal stresses, which are the boundary conditions for the tangential contact with *partial* slip. Although the way was paved to solve tangential contact problems with the method of Cattaneo and Mindlin, its application to other geometries appeared exceedingly difficult, because they required explicit knowledge/calculation of the tangential displacements. Not until 50 years later did Truman et al. [5], using this method, successfully derive the solution to the tangential contact problem between a conical indenter and an elastic half-space. In the same year, Jäger [6] arrived at the conclusion that within the framework of Cattaneo-Mindlin theory, every axially-symmetric tangential contact problem can be completely described by the normal contact problem so that an explicit calculation of the tangential displacement is unnecessary. Thereby, we remember that elastically similar materials (5.3) are assumed everywhere in this chapter, which allows the contact problem to be decoupled. Furthermore, it is assumed that the frictional stresses point in the direction of the applied tangential force, which strictly speaking, violates a part of Coulomb's law of friction. Due to the addition of a slippage component perpendicular to the applied force, the tangential stresses and slip are not opposite each other at every point in the slip domain. In [7, 8], as well as Chap. 18, it is explained why we can neglect this deviation.

Due to the principle of superposition from Jäger [6, 9], the tangential stresses are equivalent to the difference between the actual normal stress and those that correspond to a smaller contact radius (the stick radius c) multiplied with the coefficient of friction. The same is true for the tangential force F_x and the relative tangential displacement u_x:

$$\tau_{zx}(r) = \mu\left[\sigma_{zz}(a,r) - \sigma_{zz}(c,r)\right] \tag{5.18}$$

$$F_x = \mu[F_N(a) - F_N(c)] \tag{5.19}$$

$$u_x = \mu\frac{E^*}{G^*}[d(a) - d(c)]. \tag{5.20}$$

It is proven in Chap. 18 that based on the Eqs. (5.18)–(5.20), these relationships can be obtained from the method of dimensionality reduction. Thus, the method already introduced within the framework of the tangential contact for a parabolic body is generally valid. It consists primarily of two central ansätze:

1. In the one-dimensional equivalent model, the tangential spring forces at the boundary of the stick domain must assume the maximum possible value for the static frictional force

$$f_x(c) = \mu f_N(c) \qquad \Leftrightarrow \qquad q_x(c) = \mu\, q(c). \tag{5.21}$$

   For a given tangential displacement u_x, the radius of the stick domain c can be obtained.
2. The tangential force is given analogously to the normal force from the sum of the tangential spring forces and, therewith, the tangential distributed load

$$F_x = \int_{-a}^{a} q_x(x)\mathrm{d}x = 2c\, G^* u_x + 2\mu \int_{c}^{a} q(x)\mathrm{d}x. \tag{5.22}$$

   On the right side, the piecewise-defined function

$$q_x(x) = \begin{cases} G^* u_x & \text{for } |x| \le c \\ \mu\, q(x) & \text{for } c < |x| \le a \\ 0 & \text{for } |x| > a \end{cases} \tag{5.23}$$

has already been inserted.

Also, based on the superposition from Jäger, the three-dimensional tangential contact with partial slip can be replaced by two three-dimensional normal contacts. This technique has already been used in various numerical simulations. It is directly evident that such a superposition also retains its validity for the equivalent one-dimensional normal contact. Nevertheless, it is preferred, and requires less effort, to directly map the three-dimensional partial slip problem to a

one-dimensional partial slip problem, rather than mapping two three-dimensional normal contacts and superimposing them.

Now, we consider an axially-symmetric indenter which has a profile with a form given by a power function with a positive real exponent

$$\tilde{z}(r) = f(r) = C_n r^n \tag{5.24}$$

and is initially pressed into an elastic half-space with the normal force F_N and subsequently, maintaining the normal force, loaded with the tangential force F_x. We are now looking for the radius of the stick domain c and the relative tangential displacement u_x of both bodies. For the normal contact, one can take the solutions from Problem 2 in Chap. 3:

$$d(a) = C_n \kappa_n a^n \tag{5.25}$$

$$F_N(a) = \frac{2n}{n+1} E^* \kappa_n C_n a^{n+1}. \tag{5.26}$$

Let us remember that the relationships above arise from the indentation of the (rigid) profile

$$g(x) = \kappa_n C_n |x|^n, \tag{5.27}$$

which is vertically scaled by the factor κ_n, into a one-dimensional linearly elastic foundation.

The extension to the tangential contact requires that the spring elements be independent from one another in the tangential direction and possess the stiffness $\Delta k_x = G^* \Delta x$. As in the three-dimensional contact problem, Coulomb's law of friction is also locally valid in the one-dimensional model. By the addition of a tangential force, the tangential springs in the area near the edge of the contact area ($c < |x| \leq a$) slide because the vertical spring forces, and therefore, the maximum frictional forces, are locally too small to satisfy the condition $f_x(x) < \mu f_N(x)$. In this domain, the spring forces (normal and tangential) at every point are directly proportional to one another: $f_x(x) = \mu f_N(x)$. Within this radius ($|x| \leq c$), all of the tangential spring elements stick and, therefore, experience the same tangential displacement u_x. In summary, the distribution of the tangential spring forces can be expressed by means of the piecewise defined distributed load

$$q_x(x) = \begin{cases} G^* u_x & \text{for} \quad |x| \leq c \\ \mu\, E^* \kappa_n C_n (a^n - |x|^n) & \text{for} \quad c < |x| \leq a \\ 0 & \text{for} \quad |x| > a \end{cases}. \tag{5.28}$$

We determine the tangential displacement u_x as a function of the radius of the stick domain c from the condition (5.21)

$$q_x(c) = \mu q(c) \quad \Rightarrow \quad u_x(c) = \mu \frac{E^*}{G^*} \kappa_n C_n \left(a^n - c^n\right). \tag{5.29}$$

The sum of all tangential spring forces must correspond to the applied tangential force, which Eq. (5.22) provides when taking (5.29) into account:

$$F_x = \frac{2n}{n+1}\mu E^* \kappa_n C_n a^{n+1}\left[1 - \left(\frac{c}{a}\right)^{n+1}\right]. \tag{5.30}$$

Solving with respect to the characteristic ratio of the contact radii and using (5.26) leads to

$$\frac{c}{a} = \left(1 - \frac{F_x}{\mu F_N}\right)^{\frac{1}{1+n}}. \tag{5.31}$$

For $n = 2$, the result of the classical contact problem from Cattaneo and Mindlin is obtained, but also the special case of a flat, cylindrical indenter can be obtained from (5.31) if we consider $n \to \infty$. As long as the tangential force F_x is smaller than the maximum static force of friction μF_N, then the *entire* contact will stick in this case. However, if this limit is reached, then complete sliding initiates. Figure 5.2 shows Eq. (5.31) graphically for the above named geometries (paraboloid and flat indenter) as well as the conical profile ($n = 1$). The gray curve is for an exponent of $n = 6$ and signifies the family of curves for increasing n.

Using the now known radius of stick, one can also determine the tangential displacement with respect to the input values. After inserting (5.31) into (5.29) and using (5.26), it follows that

$$u_x = \frac{n+1}{2n}\frac{\mu F_N}{G^* a}\left[1 - \left(1 - \frac{F_x}{\mu F_N}\right)^{\frac{n}{n+1}}\right]. \tag{5.32}$$

Naturally, Eq. (5.32) for $n = 2$ is the result for the tangential contact of a sphere [1]. For the tangential contact between a flat, cylindrical indenter and a half-space, the limit of u_x as $n \to \infty$ must once again be found, which leads to the elementary result of

$$\lim_{n\to\infty} u_x(n) = \frac{F_x}{2G^* a}. \tag{5.33}$$

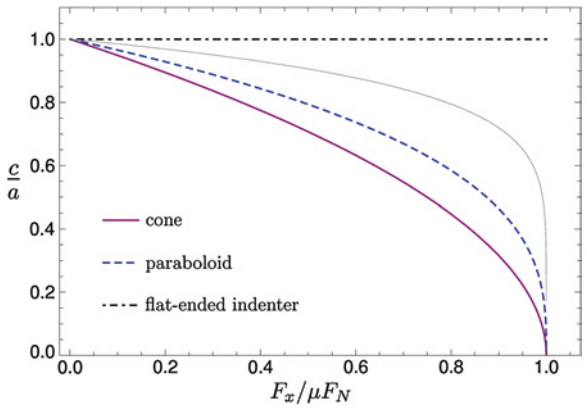

Fig. 5.2 Radius of stick c as a function of applied tangential force F_x for a conical, parabolic, and flat cylindrical indenter

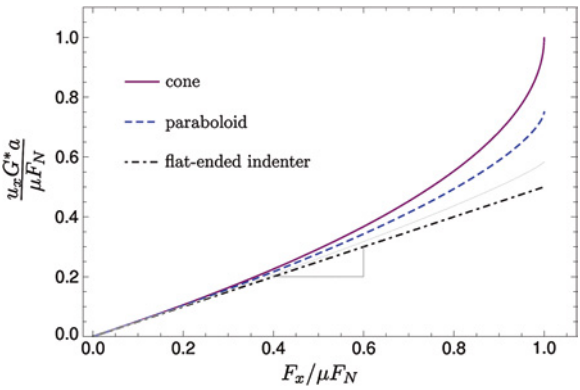

Fig. 5.3 Tangential displacement u_x plotted with respect to the tangential force F_x (normalized)

The direct proportionality between force and displacement is shown in Fig. 5.3. The slope triangle on the curve for the flat, cylindrical indenter indicates the compliance. For extremely small tangential forces, for which the slip domain is constrained to a very small ring, Eq. (5.33) is valid for all profiles, regardless of the form function exponent.

Let it once more be emphasized that the one-dimensional ansätze (5.21) and (5.22) allow for the exact mapping of tangential contacts for *arbitrary* axially-symmetric bodies. Profiles that we can describe by a *power series* as well as those that are *piecewise defined* are also included here. The latter, however, can cause difficulties, because the one-dimensional profile cannot be found simply through scaling, but must be found by integration (see Problem 3).

5.4 Mapping of Stresses in the Tangential Contact

Due to the principle of superposition from Jäger, the tangential stresses can be obtained, completely analogously to the normal stresses, from the Abel-like integral transformation of the tangential distributed load $q_x(x)$:

$$\tau_{zr}(r) = \frac{1}{\pi}\frac{1}{r}\frac{d}{dr}\int_r^a \frac{x \cdot q_x(x)}{\sqrt{x^2 - r^2}}\mathrm{d}x = \frac{1}{\pi}\int_r^a \frac{q_x'(x)}{\sqrt{x^2 - r^2}}\,\mathrm{d}x - \frac{1}{\pi}\frac{q_x(a)}{\sqrt{a^2 - r^2}}. \tag{5.34}$$

The proof for this is presented in Chap. 18. It follows from the alternate presentation of the piecewise-defined, linear force density from (5.23) as the difference between two vertical distributed loads and subsequent use of (5.18).

As an example, we want to use Eq. (5.34) on the classical tangential contact between a parabolic body and a plane. In the first step, we define the tangential

linear load for the one-dimensional model, which we already implicitly drew upon for the calculation of the tangential force in (5.15):

$$q_x(x) = \begin{cases} G^* u_x & \text{for} \quad |x| \le c \\ \mu\, E^* \left(d - \dfrac{x^2}{R} \right) & \text{for} \; c < |x| \le a \\ 0 & \text{for} \quad |x| > a \end{cases} . \tag{5.35}$$

In order to keep the effort required to a minimum, we use the integral expression on the right side of (5.34),[1] which requires the derivative of the linear load:

$$q_x'(x) = \begin{cases} 0 & \text{for } |x| \le c \;\; \vee \;\; |x| > a \\ -2\mu E^* \dfrac{x}{R} & \text{for } c < |x| \le a \end{cases} . \tag{5.36}$$

By inserting (5.36) into (5.34), we must differentiate between the two cases $0 \le r < c$ and $c \le r \le a$ and, therefore, obtain

$$\tau_{zr}(r) = -\frac{2\mu E^*}{R\pi} \cdot \begin{cases} \int\limits_c^a \dfrac{x}{\sqrt{x^2 - r^2}}\, \mathrm{d}x & \text{for } 0 \le r < c \\ \int\limits_r^a \dfrac{x}{\sqrt{x^2 - r^2}}\, \mathrm{d}x & \text{for } c \le r \le a \end{cases} . \tag{5.37}$$

After simple integration, we obtain

$$\tau_{zr}(r) = -\frac{2\mu E^*}{R\pi} \left[\sqrt{a^2 - r^2} \cdot H\left(1 - \frac{r}{a}\right) - \sqrt{c^2 - r^2} \cdot H\left(1 - \frac{r}{c}\right) \right], \tag{5.38}$$

where $H(x)$ is the Heaviside step function. It is generally known that Eq. (5.38) corresponds to the exact distribution of the tangential stress in a three-dimensional contact [1].

5.5 Mapping of Local Slip

The micro-slip in the outer area of a tangential contact is generally described by the *local* slip $s_{x,3D}(r)$. This denotes the tangential relative displacement of the surface points in the slip domain of the contact area, which is required for the calculation of wear and other tribological processes. For the sake of clarity, the constant tangential displacement of all points within the sticking domain will be denoted in the section with

$$u_x(r) = \delta_x = \text{const. for } 0 \le r \le c\,. \tag{5.39}$$

[1] Let it be noted that in special cases of non-differentiable form functions, only the first integral expression in (5.34) may be used.

The fact that this displacement can be mapped exactly by the method of dimensional reduction has already been shown. In a similar way, the local slip in the slip domain can be reproduced as

$$s_{x,3D}(r) := u_x(r) - \delta_x \text{ for } c < r \leq a\,. \tag{5.40}$$

Once again, Jäger's principle of superposition is at the center of our considerations. Using this, the following equation for the slip of an axially-symmetric contact obtained from the slip in a one-dimensional model $s_{x,1D}(x)$ can be easily understood:

$$s_{x,3D}(r) = \frac{2}{\pi} \int_0^r \frac{s_{x,1D}(x)}{\sqrt{r^2 - x^2}} \mathrm{d}x \quad \text{with} \quad s_{x,1D}(x) = u_x(x) - \delta_x. \tag{5.41}$$

Here, $u_x(x)$ is the tangential displacement of the surface of the linearly elastic foundation.

For the classical tangential contact of a parabolic body with a plane, the application of the transformation (5.41) will be explained in the following. For this, we first introduce slip in the one-dimensional model. From the tangential distributed load according to (5.35), the tangential displacements can be directly found for the equivalent system. This is because both are proportional to each other, whereby the effective shear modulus G^* is the proportionality factor:

$$u_x(x) = \begin{cases} \delta_x & \text{for} \quad |x| \leq c \\ \mu \dfrac{E^*}{G^*} \underbrace{\left(d(a) - \dfrac{x^2}{R} \right)}_{=u_z(x)} & \text{for } c < |x| \leq a\,. \end{cases} \tag{5.42}$$

With this, the following is valid for the one-dimensional slip:

$$s_{x,1D}(x) := u_x(x) - \delta_x = \begin{cases} 0 & \text{for} \quad |x| \leq c \\ \mu \dfrac{E^*}{G^*} \left(d(c) - \dfrac{x^2}{R} \right) & \text{for } c < |x| \leq a\,. \end{cases} \tag{5.43}$$

Insertion of (5.43) into (5.41) results initially in

$$s_{x,3D}(r) = \frac{2\mu E^*}{\pi R G^*} \int_c^r \frac{c^2 - x^2}{\sqrt{r^2 - x^2}} \mathrm{d}x \text{ for } c < r \leq a \tag{5.44}$$

and after simple calculation, we find the three-dimensional slip from Johnson [7] in the domain of micro-slip:

$$s_{x,3D}(r) = \frac{\mu E^*}{\pi R G^*} \left[\left(2c^2 - r^2 \right) \cdot \left(\frac{\pi}{2} - \arcsin\left(\frac{c}{r} \right) \right) - c \cdot \sqrt{r^2 - c^2} \right]. \tag{5.45}$$

5.6 Problems

Problem 1 Determine the radius of stick and the relative tangential displacement with respect to the tangential force for the tangential contact between an elastic cone and an elastic half-space. Elastically similar materials are assumed. It is also assumed that the normal contact problem for which tangential loading is investigated has already been solved (see Problem 1 in Chap. 3)

Solution The equivalent one-dimensional contact problem consists of a rigid cross-section of a conical indenter scaled vertically by a factor of $\kappa_1 = \pi/2$, which is pressed into a one-dimensional linearly elastic foundation and subsequently loaded with a tangential force. All tangential spring elements whose spring forces have not yet reached the spatially-dependent maximum static force of friction $\mu f_N(x)$ undergo the respective displacement u_x. In the outer ring, the vertical spring forces, and therefore, the force of static friction, is so small that partial sliding occurs. At the stick–slip limit, the tangential spring forces must assume the maximum force of static friction

$$G^* \Delta x \, u_x(c) = \mu \, E^* \Delta x \big[d - g(c) \big], \tag{5.46}$$

which results in *constant* tangential displacement of all points in the stick domain:

$$u_x(x) = \mu \frac{\pi}{2} \frac{E^* \tan\theta}{G^*} (a - c) \quad \text{for} \quad |x| \le c. \tag{5.47}$$

In equilibrium, the tangential force F_x must be equal to the sum of the tangential spring forces:

$$\begin{aligned} F_x &= G^* \int_{-a}^{a} u_x(x) \, \mathrm{d}x = 2G^* \int_{0}^{c} u_x(x) \, \mathrm{d}x + 2\mu E^* \int_{c}^{a} u_z(x) \, \mathrm{d}x \\ &= \frac{\pi}{2} \mu E^* \tan(\theta) \, a^2 \left[1 - \left(\frac{c}{a} \right)^2 \right]. \end{aligned} \tag{5.48}$$

By taking the results of the normal contact problems into account (see Problem 1 from Chap. 3), Eqs. (5.47) and (5.48) can be brought into the following form:

$$\frac{c}{a} = \sqrt{1 - \frac{F_x}{\mu F_N}} \tag{5.49}$$

$$u_x = \frac{\mu F_N}{G^* a} \left[1 - \sqrt{1 - \frac{F_x}{\mu F_N}} \right]. \tag{5.50}$$

Of course, these equations also result from (5.31) and (5.32) for $n = 1$ and correspond exactly with the three-dimensional solution from Truman et al. [5].

Problem 2 Calculate the tangential stress distribution within the contact area for the tangential contact handled in Problem 1 with the help of the Abel transformation in Eq. (5.34).

Solution The calculation of the three-dimensional tangential stress from the one-dimensional model requires setting up the equation for and subsequently differentiating the tangential linear load. The linear load was already implicitly used to find the tangential force in Eq. (5.48). Its derivative is

$$q'_x(x) = \begin{cases} 0 & \text{for } |x| \le c \quad \text{and} \quad |x| > a \\ -\mu E^* \frac{\pi}{2} \tan\theta \cdot \operatorname{sign}(x) & \text{for } c < |x| \le a \end{cases} . \tag{5.51}$$

Inserting (5.51) into Eq. (5.34) initially provides

$$\tau_{zr}(r) = -\frac{1}{2}\mu E^* \tan\theta \cdot \begin{cases} \int_c^a \frac{1}{\sqrt{x^2 - r^2}}\,\mathrm{d}x & \text{for } 0 \le r < c \\ \int_r^a \frac{1}{\sqrt{x^2 - r^2}}\,\mathrm{d}x & \text{for } c \le r \le a \end{cases} , \tag{5.52}$$

and after integration and simple rearrangement,

$$\tau_{zr}(r) = -\frac{1}{2}\mu E^* \tan\theta \left[\operatorname{arcosh}\left(\frac{a}{r}\right) \cdot H\left(1 - \frac{r}{a}\right) - \operatorname{arcosh}\left(\frac{c}{r}\right) \cdot H\left(1 - \frac{r}{c}\right)\right]. \tag{5.53}$$

The tangential stress distribution, normalized by the mean value in the case of complete sliding, is plotted in Fig. 5.4 for sizes of the stick domain. The finite value at the point $r = 0$ is

$$\lim_{r\to 0} \frac{-\tau_{zr}(r)}{\mu p_m} = \lim_{r\to 0} \left[\operatorname{arcosh}\left(\frac{a}{r}\right) - \operatorname{arcosh}\left(\frac{c}{r}\right)\right] = \lim_{r\to 0} \ln\left(\frac{a + \sqrt{a^2 - r^2}}{c + \sqrt{c^2 - r^2}}\right) = \ln\left(\frac{a}{c}\right). \tag{5.54}$$

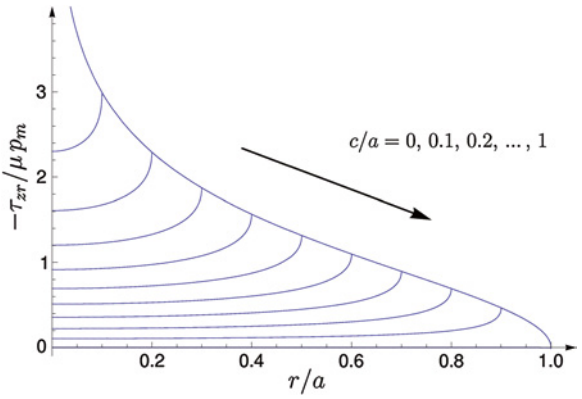

Fig. 5.4 Normalized tangential stress distribution with respect to the size of the stick domain $c/a = 0.1, 0.2, \ldots, 1$

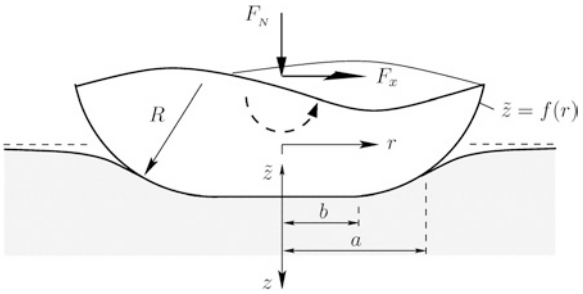

Fig. 5.5 Tangential contact of a flat indenter with rounded edges (radius R)

Problem 3 A flat, cylindrical indenter with rounded edges is initially pressed into an elastic half-space with the normal force F_N and subsequently loaded with a (presently unknown) tangential force F_x, which results in a given relative tangential displacement u_x of the two bodies. It is assumed that the bodies are composed of elastically similar materials and that the profile of the indenter is given by the following (see Fig. 5.5):

$$f(r) = \begin{cases} 0 & \text{for } 0 \le r < b \\ \frac{1}{2R}(r-b)^2 & \text{for } b \le r \le a \end{cases}. \tag{5.55}$$

Determine the indentation depth and normal force as a function of contact radius with the help of the reduction method. Furthermore, calculate the tangential displacement and tangential force as a function of the stick radius.

Solution In the first step, the one-dimensional equivalent profile must be determined. The piecewise-defined function according to (5.55) requires the application of the generalized formula (3.27)

$$g(x) = x \int_0^x \frac{f'(r)}{\sqrt{x^2 - r^2}} \mathrm{d}r = \begin{cases} 0 & \text{for } 0 \le x < b \\ \frac{x}{R} \int_b^x \frac{r-b}{\sqrt{x^2 - r^2}} \mathrm{d}r & \text{for } b \le x \le a \end{cases}. \tag{5.56}$$

Calculating the integral in Eq. (5.56) requires nothing more than elementary mathematics:

$$\int_b^x \frac{r-b}{\sqrt{x^2 - r^2}} dr = \sqrt{x^2 - b^2} - b \arccos\left(\frac{b}{x}\right). \tag{5.57}$$

Nevertheless, we must remember that (5.56) has to be extended axis-symmetrically to the domain of $-a \le x \le 0$. Then, we obtain

$$g(x) = \begin{cases} 0 & \text{for } \quad |x| < b \\ \frac{|x|}{R}\sqrt{x^2 - b^2} - \frac{b|x|}{R} \arccos\left(\frac{b}{|x|}\right) & \text{for } b \le |x| \le a \end{cases}. \tag{5.58}$$

The normalized original and equivalent profiles are shown in Fig. 5.6.

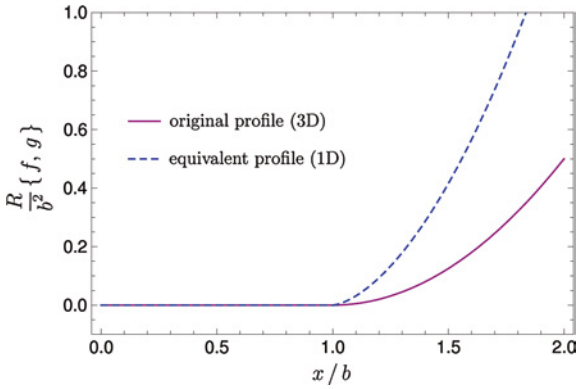

Fig. 5.6 Flat indenter with rounded edges: Comparison between the three-dimensional and one-dimensional profiles

The indentation depth as a function of the contact radius is found from the one-dimensional profile using

$$d = g(a) = \frac{a}{R}\sqrt{a^2 - b^2} - \frac{ba}{R}\arccos\left(\frac{b}{a}\right), \tag{5.59}$$

while the dependence of the normal force on the contact radius is found from the sum of all spring forces in the contact for the one-dimensional model:

$$\begin{aligned} F_N &= 2E^* \int_0^a \left[d - g(x)\right] \mathrm{d}x \\ &= 2E^* \int_0^b d \, \mathrm{d}x + 2E^* \int_b^a \left[d - \left(\frac{x}{R}\sqrt{x^2 - b^2} - \frac{bx}{R}\arccos\left(\frac{b}{x}\right)\right)\right] \mathrm{d}x. \end{aligned} \tag{5.60}$$

Integration, taking (5.59) into account, and rearranging results in

$$F_N = \frac{4}{3}E^*\frac{a^3}{R}\left[\left(1 - \frac{1}{4}\left(\frac{b}{a}\right)^2\right)\sqrt{1 - \left(\frac{b}{a}\right)^2} - \frac{3}{4}\frac{b}{a}\arccos\left(\frac{b}{a}\right)\right]. \tag{5.61}$$

The limiting case of $b = 0$ is a parabolic profile. As expected, the Eqs. (5.59) and (5.61) reproduce in this limit the Hertzian relations.

The boundary between slip and stick can be found using Eq. (5.21), in other words, requiring that the tangential spring force reaches the maximum possible force of static friction at the point $x = c$. With the help of (5.58) and (5.59), one of the relationships is found:

$$u_x = \mu\frac{E^*}{G^*}\frac{a}{R}\left[\sqrt{a^2 - b^2} - b\arccos\left(\frac{b}{a}\right) - \frac{c}{a}\left(\sqrt{c^2 - b^2} - b\arccos\left(\frac{b}{c}\right)\right)\right]. \tag{5.62}$$

Now, it is only left to find the dependence between the tangential force and the stick radius. For this, we look at a distributed load in the one-dimensional model

$$q_x(x) = \begin{cases} G^* u_x & \text{for} \quad |x| \le c \\ \mu E^* \left[d - \dfrac{|x|}{R} \left(\sqrt{x^2 - b^2} - b \arccos\left(\dfrac{b}{|x|} \right) \right) \right] & \text{for} \quad c < |x| \le a \\ 0 & \text{for} \quad |x| > a \end{cases} \tag{5.63}$$

and integrate this over the contact width in the reduced model:

$$F_x = \int_{-a}^{a} q_x(x) \mathrm{d}x = 2cG^* u_x + 2\mu E^* \int_{c}^{a} \left[d - \frac{x}{R} \left(\sqrt{x^2 - b^2} - b \arccos\left(\frac{b}{x} \right) \right) \right] \mathrm{d}x. \tag{5.64}$$

The integral on the right-hand side already appeared in the calculation of the normal force in (5.60). After calculating the antiderivative and taking the lower limit of integration into account, we obtain

$$\begin{aligned} F_x = {} & \mu \frac{E^*}{3R} \left[\left(4a^2 - b^2 \right) \sqrt{a^2 - b^2} - 3a^2 b \arccos\left(\frac{b}{a} \right) \right] \\ & - \mu \frac{E^*}{3R} \left[\left(4c^2 - b^2 \right) \sqrt{c^2 - b^2} - 3c^2 b \arccos\left(\frac{b}{c} \right) \right]. \end{aligned} \tag{5.65}$$

We can be directly convinced of the correctness of Eq. (5.65) if we consider the principle of superposition by Jäger. According to (5.19), the tangential force is equivalent to the difference between the current normal force and one that would result in a stick radius c multiplied by the coefficient of friction. Using Eq. (5.61), this relationship can be easily verified. Figure 5.7 shows the normalized dependence of the stick radius on the tangential force for various cases. The limiting case of $b = 0$ corresponds to the classical result of Cattaneo and Mindlin. In contrast, if the contact area is only slightly larger than the flat section ($b = 0.95a$), then the curve approaches that of a flat indenter. A comparison is shown in Fig. 5.2.

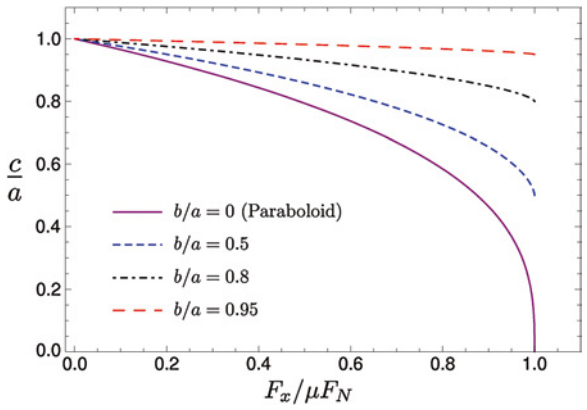

Fig. 5.7 Stick radius c as a function of applied tangential force F_x for a flat indenter with rounded edges

Although it has not yet been mentioned, it was assumed in the above calculations that $b \leq c \leq a$, and therefore, partial sliding within the flat section is not possible. Figure 5.7 emphasizes the validity of this assumption. As soon as the slip domain includes the rounded edges, then the transition to complete slip takes place. For the analogous planar contact problem, a corresponding behavior was analytically proven [10] and verified by finite element calculations [11].

Problem 4 Determine the integral form for the normal and tangential stress distribution for the contact between a flat indenter with rounded edges having a radius of curvature of R and a half-space (see Fig. 5.5). Assume a constant distributed loading of the one-dimensional model and visualize the numeric solutions of the integral expressions.

Solution The vertical distributed load in the one-dimensional model is directly proportional to the normal displacement of the surface and according to Eq. (5.58) is

$$q(x) = \begin{cases} d & \text{for} \quad |x| \leq b \\ E^* \left[d - \dfrac{|x|}{R} \left(\sqrt{x^2 - b^2} - b \arccos\left(\dfrac{b}{|x|} \right) \right) \right] & \text{for} \quad b < |x| \leq a \\ 0 & \text{for} \quad |x| > a \end{cases} . \tag{5.66}$$

The derivative is required for the calculation of the normal stress distribution. Because of axial symmetry, we only have to determine this for positive x:

$$q'(x) = \begin{cases} 0 & \text{for } 0 \leq x < b \ \vee \ x > a \\ -\dfrac{E^*}{R} \left[2\sqrt{x^2 - b^2} - b \arccos\left(\dfrac{b}{x} \right) \right] & \text{for} \quad b \leq x \leq a \end{cases} . \tag{5.67}$$

According to Eq. (3.37) from Chap. 3, the normal stress is

$$\sigma_{zz}(r) = \begin{cases} -\dfrac{E^*}{\pi R} \displaystyle\int_b^a \dfrac{2\sqrt{x^2 - b^2} - b \arccos(b/x)}{\sqrt{x^2 - r^2}} \, \mathrm{d}x & \text{for } 0 \leq r < b \\ -\dfrac{E^*}{\pi R} \displaystyle\int_r^a \dfrac{2\sqrt{x^2 - b^2} - b \arccos(b/x)}{\sqrt{x^2 - r^2}} \, \mathrm{d}x & \text{for } b \leq r \leq a \end{cases} . \tag{5.68}$$

These integral relations are identical to those of the three-dimensional theory. They must be solved numerically. Figure 5.8 shows the distribution of the normal stress in normalized form, where $p_m := F_N / \pi a^2$ is the mean stress. Several ratios of the length of the flatness b and the contact radius a are shown. For $b = 0$, we understandably obtain the Hertzian results, while for $b \to a$, we obtain the singularity at the edges of the contact for a flat, cylindrical indenter (with sharp edges). The presence of rounded edges guaranties a finite maximum in stress, which decreases with b/a towards the center.

The calculation of the tangential stress follows completely analogously. The tangential distributed load of the linearly elastic foundation was already shown in Problem 3 so that we must now only focus on $0 \leq x \leq a$ and differentiate (5.63) with respect to x:

$$q_x'(x) = \begin{cases} 0 & \text{for } 0 \leq x < c \ \vee \ x > c \\ -\dfrac{\mu E^*}{R} \left[2\sqrt{x^2 - b^2} - b \arccos\left(\dfrac{b}{x} \right) \right] & \text{for} \quad c \leq x \leq a \end{cases} . \tag{5.69}$$

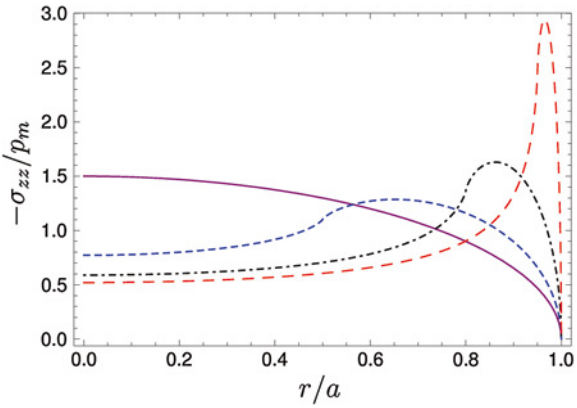

Fig. 5.8 Distribution of the normalized stress for the contact in Fig. 5.5; the cases shown are those from Problem 3: $b/a = 0$ (Hertzian pressure distribution) as well as $b/a = 0.5,\ 0.8,$ and 0.95

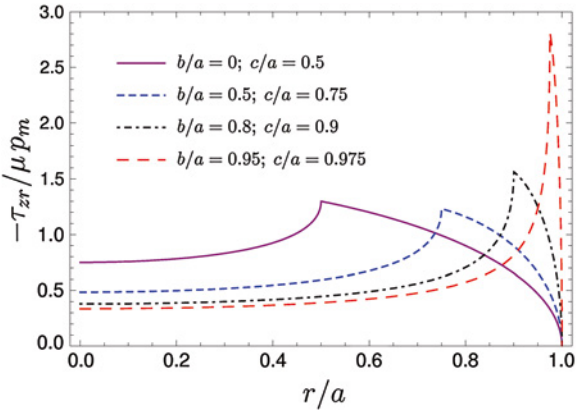

Fig. 5.9 Distribution of the tangential stress for the chosen values; the values are normalized by the average tangential stress in the case of complete sliding

Insertion of (5.69) into (5.34) results in the distribution of the tangential stress in integral form, which corresponds to (5.68) with the exception of the integral boundaries:

$$\tau_{zr}(r) = \begin{cases} -\dfrac{\mu E^*}{\pi R} \displaystyle\int_c^a \dfrac{2\sqrt{x^2 - b^2} - b \arccos(b/x)}{\sqrt{x^2 - r^2}}\, \mathrm{d}x & \text{for } 0 \le r < c \\ -\dfrac{\mu E^*}{\pi R} \displaystyle\int_r^a \dfrac{2\sqrt{x^2 - b^2} - b \arccos(b/x)}{\sqrt{x^2 - r^2}}\, \mathrm{d}x & \text{for } c \le r \le a \end{cases} . \quad (5.70)$$

Numerically solving (5.70) leads to the normalized trend in Fig. 5.9 for the chosen values $b \le c \le a$. A comparison with Fig. 5.8 allows the principle of superposition from Jäger to be clearly seen; especially for $b = 0$ and the arbitrarily chosen ratio of stick to contact radius $c/a = 0.5$, the classical solution from Cattaneo and Mindlin is evident.

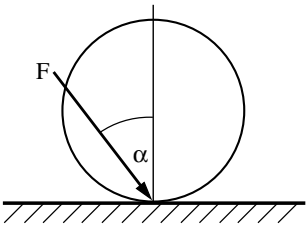

Fig. 5.10 Elastic sphere that is pressed by an inclined force onto a rigid half-space

The equations for the normal and tangential stresses according to (5.68) and (5.70) obtained from the distributed load in the one-dimensional model, occur identically in the three-dimensional theory [12].

Problem 5 An elastic sphere is pressed onto a rigid half-space, for which the direction of the indentation force always remains the same (Fig. 5.10). Determine the conditions under which the entire contact area sticks.

Solution In contrast to the three-dimensional case, the solution is trivial within the framework of the reduction method. Due to the fact that every sticking spring is loaded by the angle α, there is no sliding if the angle is smaller than the frictional angle [1]:

$$\tan\alpha < \mu. \tag{5.71}$$

The result is, as expected, exactly the same as that for the three-dimensional solution.

Problem 6 *Fretting wear*. Consider a rotationally symmetric profile which is brought into contact with a rigid surface and then oscillates in tangential direction with a given amplitude $u_x^{(0)}$. For small oscillation amplitudes, the wear occurs only in a circular slip zone at the border of the contact area. With increasing number of cycles, the wear profile tends to a limiting form, in which no further wear occurs. Under assumption of a constant coefficient of friction, the limiting form of the wear profile does not depend on the particular wear criterion. Using the method of dimensionality reduction, determine analytically this limiting form (for details see [13]).

Solution Assume that the friction can be described by a local formulation of the Amonton's law: The surfaces in contact are in the sticking state if tangential stress τ is smaller than normal pressure p multiplied with a constant coefficient of friction μ, and the tangential stress remains constant after the onset of sliding:

$$\begin{array}{l} \tau < \mu p, \text{ stick} \\ \tau = \mu p, \text{ slip} \end{array}. \tag{5.72}$$

At the circular border of the stick region with radius c, the critical condition $\tau(c) = \mu p(c)$ is fulfilled. Inside this region, the condition $\tau < \mu p$ is valid. Due to wear outside of the sticking region, the local pressure in the sticking region will increase and outside decrease further, independently of whether the experiment is

done under conditions of constant normal force or constant indentation depth d. This will lead to a progressive wear outside of the region of stick. The wear process will advance until the pressure in the sliding region becomes zero. In this limiting state, the inner parts of the contact will still remain in the sticking state, while the wear rate in the outer parts of the contact tends to zero. The final state of no wear can be considered as a sort of "shakedown" state, in which no further inelastic processes occur. The detailed kinetics of the profile depends on the wear criterion used as well as on the loading conditions (controlled force or controlled indentation). In the most cases, the Reye-Archard-Khrushchov wear criterion is used, stating that the wear volume is proportional to the dissipated energy. According to this wear criterion, the wear rate vanishes if either the relative displacement Δu_x of the bodies or tangential stress in contact is zero. In non-adhesive contacts, the latter means vanishing of the normal pressure p. The no-wear condition thus reads:

$$\text{No wear condition:} \begin{cases} \text{either} & p = 0 \\ \text{or} & \Delta u_x = 0 \end{cases}. \tag{5.73}$$

From these conditions, it follows that the pressure in the final state is non-zero only inside the stick area and vanishes outside.

Given a three-dimensional profile $z = f(r)$, we first determine the equivalent one-dimensional profile according to (3.27)

$$g(x) = |x| \int_0^{|x|} \frac{f'(r)}{\sqrt{x^2 - r^2}} \mathrm{d}r. \tag{5.74}$$

The back transformation is given by the integral

$$f(r) = \frac{2}{\pi} \int_0^r \frac{g(x)}{\sqrt{r^2 - x^2}} \mathrm{d}x. \tag{5.75}$$

The profile (5.74) is pressed to a given indentation depth d into an elastic foundation. The resulting vertical displacements of springs are given by

$$u_z(x) = d - g(x) \tag{5.76}$$

and the linear force density

$$q(x) = E^* u_z(x) = E^*(d - g(x)). \tag{5.77}$$

The contact radius a is given by the condition

$$g(a) = d. \tag{5.78}$$

The distribution of normal pressure $p = -\sigma_{zz}$ in the initial three-dimensional problem can be calculated using the integral transformation (3.37):

$$p(r) = -\frac{1}{\pi}\int_r^\infty \frac{q'(x)}{\sqrt{x^2 - r^2}}\mathrm{d}x = \frac{E^*}{\pi}\int_r^\infty \frac{g'(x)}{\sqrt{x^2 - r^2}}\mathrm{d}x. \tag{5.79}$$

If the profile is moved tangentially by $u_x^{(0)}$, the springs will be stressed both in the normal and tangential direction, and the radius c of the stick region will be given by the condition that the tangential force $k_x u_x^{(0)}$ is equal to the coefficient of friction μ multiplied with the normal force $k_z u_z(c)$:

$$G^* u_x^{(0)} = \mu E^*(d - g(c)). \tag{5.80}$$

Let us denote the initial three-dimensional profile as $f_0(r)$, the corresponding one-dimensional image as $g_0(x)$ and the limiting shakedown shapes as $f_\infty(r)$ and $g_\infty(x)$ correspondingly. As discussed above, the pressure outside the stick area must vanish in the limiting shakedown state: $p(r) = 0$, for $r > c$. From (5.79), it follows that

$$g'(x) = 0 \quad \text{and} \quad g(x) = const = g_0, \quad \text{for } c < x < a. \tag{5.81}$$

From the condition (5.76), it then follows that the one-dimensional profile in the shakedown state has the form

$$g_\infty(x) = \begin{cases} g_0(x), & \text{for } 0 < x < c \\ d, & \text{for } c < x < a \end{cases}. \tag{5.82}$$

This shape is schematically shown in Fig. 5.11. The three-dimensional limiting shape can now be calculated by the back transformation (5.75):

$$f_\infty(r) = \begin{cases} f_0(r) & \text{for } 0 < r < c \\ \dfrac{2}{\pi}\displaystyle\int_0^c \frac{g_0(x)}{\sqrt{r^2 - x^2}}\mathrm{d}x + \frac{2}{\pi}d\int_c^r \frac{1}{\sqrt{r^2 - x^2}}\mathrm{d}x, & \text{for } c < r < a \end{cases}. \tag{5.83}$$

Let us apply Eq. (5.83) to a parabolic indenter. In this case, the initial profile is $f_0(r) = r^2/(2R)$, and the corresponding one-dimensional MDR-image is $g_0(x) = x^2/R$. The radius of the stick region is given by the condition (5.80):

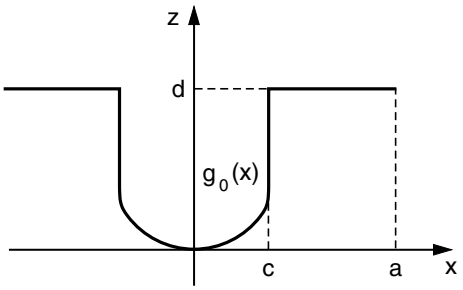

Fig. 5.11 One-dimensional MDR-image of the final "shakedown" profile

$$c = \sqrt{R\left(d - \frac{G^*}{E^*}\frac{u_x^{(0)}}{\mu}\right)}. \tag{5.84}$$

According to (5.83), the limiting three-dimensional profile has the form

$$f_\infty(r) = \begin{cases} \dfrac{r^2}{2R}, & \text{for } 0 < r < c \\ d - \dfrac{2}{\pi}\left(d - \dfrac{r^2}{2R}\right)\arcsin\dfrac{c}{r} - \dfrac{r^2}{\pi R}\left(\dfrac{c}{r}\right)\sqrt{1-\left(\dfrac{c}{r}\right)^2}, & \text{for } c < r < a \end{cases}. \tag{5.85}$$

Normalizing all vertical coordinates by the indentation depth d and horizontal coordinates by the contact radius of the initial profile, $a_0 = \sqrt{Rd}$,

$$\begin{aligned} &\tilde{f} = f/d, \quad \tilde{d} = d/d = 1 \\ &\tilde{r} = r/a_0, \quad \tilde{x} = x/a_0, \quad \tilde{c} = c/a_0, \quad \tilde{a} = a/a_0, \end{aligned} \tag{5.86}$$

we can rewrite these equations in the dimensionless form

$$\tilde{f}_\infty(\tilde{r}) = \begin{cases} \dfrac{\tilde{r}^2}{2}, & \text{for } 0 < \tilde{r} < \tilde{c} \\ 1 - \dfrac{2}{\pi}\left(1 - \dfrac{\tilde{r}^2}{2}\right)\arcsin\dfrac{\tilde{c}}{\tilde{r}} - \dfrac{\tilde{r}\tilde{c}}{\pi}\sqrt{1-\left(\dfrac{\tilde{c}}{\tilde{r}}\right)^2}, & \text{for } \tilde{c} < \tilde{r} < \tilde{a} \end{cases}. \tag{5.87}$$

The non-dimensional form of the limiting profile thus depends only on one parameter $0 < \tilde{c} < 1$. The contact radius, and thus the outer radius of the wear region, is given by the condition $\tilde{f}_\infty(\tilde{a}) = \tilde{f}_0(\tilde{a})$:

$$1 - \frac{2}{\pi}\left(1 - \frac{\tilde{a}^2}{2}\right)\arcsin\frac{\tilde{c}}{\tilde{a}} - \frac{\tilde{a}\tilde{c}}{\pi}\sqrt{1-\left(\frac{\tilde{c}}{\tilde{a}}\right)^2} = \frac{\tilde{a}^2}{2}. \tag{5.88}$$

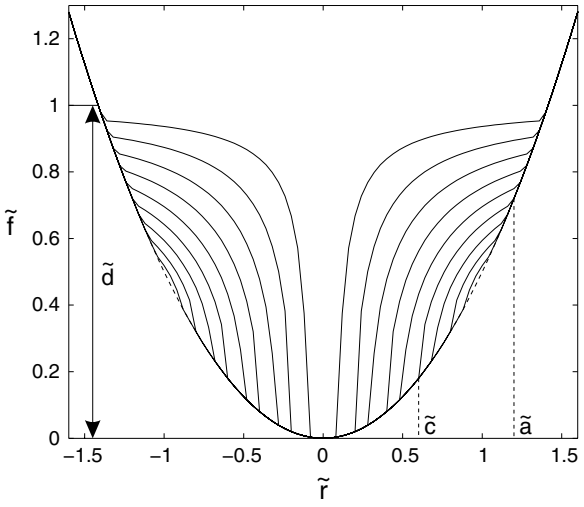

Fig. 5.12 3D profiles in the final state according to Eq. (5.87). Parameters: 9 linearly increasing $\tilde{c}$ from 0.1 to 0.9

In the limiting case $\tilde{c} = 0$, the contact radius becomes $\tilde{a} = \sqrt{2}$.

The total force can be calculated as

$$F_N = 2\int_0^a E^*(d - g(x))\mathrm{d}x = 2\int_0^c E^*\left(d - x^2\Big/R\right)\mathrm{d}x = 2E^*\left(dc - \frac{c^3}{3R}\right) \quad (5.89)$$

or, under consideration of (5.84),

$$F_N = \frac{4}{3}E^*R^{1/2}\left(d - \frac{G^*}{E^*}\frac{u_x^{(0)}}{\mu}\right)^{1/2}\left(d + \frac{G^*}{2E^*}\frac{u_x^{(0)}}{\mu}\right). \quad (5.90)$$

Profiles (5.87) are shown in Fig. 5.12 for a representative set of parameters.

References

1. V.L. Popov, *Contact Mechanics and Friction. Physical Principles and Applications* (Springer, Berlin, 2010)
2. K.L. Johnson, *Contact Mechanics* (Cambridge University Press, Cambridge, 1985). (Chap. 7)
3. C. Cattaneo, Sul contatto di due corpi elastici: distribuzione locale degli sforzi. Rendiconti dell'Accademia nazionale dei Lincei. **27**, 342–348, 434–436, 474–478 (1938)
4. R.D. Mindlin, Compliance of elastic bodies in contact. J. Appl. Mech. **16**(3), 259–268 (1949)
5. C.E. Truman, A. Sackfield, D.A. Hills, Contact mechanics of wedge and cone indenters. Int. J. Mech. Sci. **37**(3), 261–275 (1995)
6. J. Jäger, Axi-symmetric bodies of equal material in contact under torsion or shift. Arch. Appl. Mech. **65**, 478–487 (1995)
7. K.L. Johnson, Surface interaction between elastically loaded bodies under tangential forces. Proc. R. Soc. **A230**, 531 (1955)
8. R.L. Munisamy, D.A. Hills, D. Nowell, Static axisymmetric hertzian contacts subject to shearing forces. ASME J. Appl. Mech. **61**, 278–283 (1994)
9. J. Jäger, A new principle in contact mechanics. J. Tribol. **120**(4), 677–684 (1998)
10. M. Ciavarella, D.A. Hills, G. Monno, The influence of rounded edges on indentation by a flat punch. J. Mech. Eng. Sci., Proc. Inst. Mech. Eng. Part C **212**(4), 319–328 (1998)
11. J. Jäger, New analytical solutions for a flat rounded punch compared with FEM. Comput. Methods Contact Mech. V, 307–316 (2001)
12. M. Ciavarella, Indentation by nominally flat or conical indenters with rounded corners. Int. J. Solids Struct. **36**, 4149–4181 (1999)
13. V.L. Popov, Analytic solution for the limiting shape of profiles due to fretting wear. Sci. Rep. **4**, 3749 (2014). doi:10.1038/srep03749

http://www.springer.com/978-3-642-53875-9

Method of Dimensionality Reduction in Contact Mechanics and Friction

Popov, V.; Heß, M.

2015, XVII, 265 p. 115 illus., 13 illus. in color., Hardcover
ISBN: 978-3-642-53875-9